Tel Aviv University

The Raymond and Beverly Sackler Faculty of Exact Sciences

School of Physics and Astronomy

Enhancing optical nonlinearity by controlling the ultrafast dynamics in plasmonic nanostructures

Thesis submitted in partial fulfillment of the requirements for M.Sc. at Tel-Aviv University

by

Achiya Nagler

This work was carried out under the supervision of

Dr. Haim Suchowski

November, 2016

Contents

Acknowledgments

I would like to thank my family for their love and support. My son's passion in exploring the world and his willingness to help me in the middle of the nights to create new physics models inspired me a lot.

I would also like to thank my adviser, Dr. Haim Suchowski, for all the help, guidance and the interesting discussions on the models over the past two years.

Lastly, I would like to thank the pioneers of the 'SHG' group which started the journey toward the unexplored 'fs-nm-IR' physics.

1 Abstract

The main goal of my research was to determine whether pulse shaping of an incoming pulse can enhance the nonlinear optical response of a plasmonic nanostructures. For that, I have performed research in several fronts: the nanostructures world, ultrafast dynamics and coherent control.

As part of my work, we have built a pulse shaper based on a Spatial Light Modulator (SLM) and a Frequency-Resolved Optical Gating (FROG) characterization tool. Both tools allow us to control and charactrize ultrafast phenomena in the femtosecond time scale. Moreover, we have verified the calibration by employing coherent control techniques.

We have developed theoretical understanding on nanostructures' phenomena using plasmonics theories and expanded the common models to fit our laboratory's measurement-scenarios. The expanded models where used to explain the effect of thin layers on plasmon's resonance. Moreover, we theoretically showed that coherent control can increase nonlinearity in plasmonic systems.

I have written numerical simulation of the Two-Temperature Model (TTM) to validate the phase dependecy of ultrafast dynamics in plasmonic system. Using coherent control techniques, it was shown that the temperature of the electrons can be controlled by only changing the phase of the pulse's energy absorbed in the system. This phenomenon can be measured using pump-probe technique combined with an SLM, as suggested in the text.

2 Introduction

The femto(second)-nano(meter) field comes to explain the interaction between ultrashort laser pulses and nanometer scale plasmonic systems. Femtonano applications can be used in devices such as photodetector and "solar cells" technologies [1]. The goal of my research is to study ultrafast phenomena at nanoscale resolution via coherent control methods.

Ultrafast phenomena in plasmonic nanostructures has been extensively studied in the last few years. We want to study the photo-induced ultrafast dynamics in plasmonic nanostructures which displays different temperatures for the electrons and lattice at the femtosecond time scale caused by an incoming pulse. This phenomena was not yet explored via coherent control methods. Coherent control can be achieved through pulse-shaping which is obtained by tailoring the spectral phase of the excitation pulse. The theoretical model I used for exploring the temporal effects is mainly based on the Two Temperature Model (TTM) which describes the temperatures of the electrons and the lattice with a femtosecond resolution while and after a laser pulse is absorbed.

During the theoretical studies we built tools for exploring the femtosecond-nanoscale (fs-nm) phenomena, such as Second Harmonic Generation Frequency Resolved Optical Gating (SHG FROG), a pulse-shaper and more, where I mainly created automation of the measurements and the data processing of the results.

This study is organized as follows: In chapter 3, I present some relevant theories about the nm-world and about the fs-world. Chapter 4 reports the key results of my M.Sc, where I introduce some new models for the effects of coherent control on plasmonic system. Finally, we present a model which describes the time evolution of electronic temperature in plasmonic systems and demonstrate how the temperature's dynamics can be controlled via pulse shaping In the appendix I describe approaches made in models of plasmonic systems with thin layer.

"For every complex problem there is an answer that is clear, simple, and wrong."

H. L. Mencken

3 Background

3.1 Nanometer scale phenomena

3.1.1 Introduction to nanoscale physics in metals

Plasmonic waves are waves of free electrons in a metal, created due to interaction with electromagnetic (EM) radiation, as can be seen in figure [3.1]. Light is highly confined in the nano-space and consequently optical field enhanced locally, leading to various novel optical phenomena including: super-resolution optical imaging, nano-lithography, and it enables multiphoton-induced chemical reactions and photo-electron emission which is well suited for potential applications in nanophotonic devices, molecular sensors and photo-voltaic devices.

In the nanoscale regime, a metallic nanostructure (NS) is very small compared to the wavelength and the skin-penetration-depth of the electric-field. Consequently, during an interaction between metallic-matter and an electric-field, the field penetrates into the NS and induces a spatial field which creates a metal-polarization (different from electric field-polarization) by displacing the metal's electrons in the opposite direction of the electric field, towards the metal/dielectric separating surface. The metal-polarization strength depends on the following components: the geometry of the NS, the metal constructing the NS, the permittivity of the dielectric medium surrounding the NS, the fraction of the NS in the medium, the wavelength and the electric field-polarization [2].

In order to model the interaction between an electric field and a NS, a semi-classical method can be implemented for evaluating the induced total polarizability which is used for deriving the collective optical behavior of the plasmonic system, such as absorption, scattering and extinction cross-sections, as will be shown next.

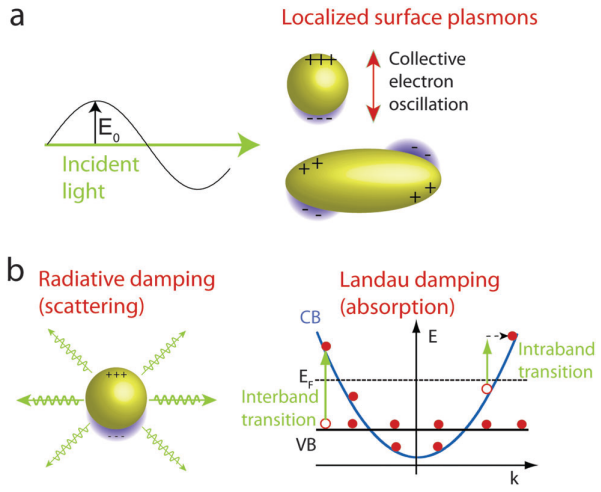

Figure 3.1: (a) Schematic electron displacement associated to the localized surface plasmon resonance of a metal nanoparticle: a collective displacement is induced by an incident light beam for an object much smaller than the light wavelength, resulting in a dipolar response, while a non-uniform displacement occurs for nano-objects with a larger size along the propagation direction of the incident light wave, exciting higher-order plasmon modes. (b) Plasmon decay mechanisms via radiative (elastic scattering of the incident light) and non-radiative (Landau damping, i.e., single electron–hole excitations) processes. The latter can take place by intraband (a conduction band, CB, electron is excited to an unoccupied CB state) or interband (excitation of a valence band, VB, electron in the CB) transitions. [3]

3.1.2 Effective medium theory: Maxwell-Garnett Theory

Effective medium theory (EMT) [4] [5] [6] pertains to analytical or theoretical modeling that describes the macroscopic properties of composite materials based on the properties and the relative fractions of its components. Maxwell-Garnett Theory (MGT) is an EMT method for calculating the plasmon's collective properties and the local surface plasmon resonance (LSPR) created by a combination of a small metal fraction in a dielectric medium [1]. The advantage of the method is mostly seen when solving Maxwell's equations becomes practically impossible, e.g an in-homogeneity composite where metal and dielectric components intersperse with each other in a disordered manner. The collective properties can be deduced by evaluating the effective dielectric function, ϵ_{eff}, of the microscopically uniform medium. ϵ_{eff} can be obtained as a function of the permittivity, ϵ, and polarizability, α, of the individual components combined with there respective volume fractions, f. This method is known as the effective medium approach.

We shall start the analysis by looking at the local field inside the metallic NS, E_L, that is induced by an external field in the NS as in figure [3.2] . $E_L = E_0 + E_d + E_S + E_{near}$,

[1] Besides MGT's effective medium theory that we shall focus on, the published literature on composites contains a range of other mixing rules including Bruggeman's, Polder and van Santen's methods [7]

where:

E_0-The external electric field

E_d-Depolarization field due to the charges of macroscopic polarization, P, lying at the external surface of the medium. $E_d = -P/(\epsilon_h \cdot \epsilon_0)$, where ϵ_h is the host permittivity.[2]

E_S-The field due to the polarization charges lying on the surface as can be seen in figure [3.2] for Lorentz Sphere. $E_S = \frac{L_i}{\epsilon_0 \epsilon_h} P$ where L_i is a geometry dependent unit-less factor for the i-axis where $0 \leq L_i \leq 1$, where a_i, a_j and a_k are the semi-axes of the ellipsoidal particle:

$$L_{\mathrm{i}} = \frac{a_1 a_2 a_3}{2} \int_0^\infty \frac{1}{(s+a_i^2)^{3/2}(s+a_j^2)^{1/2}(s+a_k^2)^{1/2}} ds \tag{3.1}$$

$E_{near}-$The field induced by other dipoles lying within the sphere. Here we assume $E_{near} = 0$.

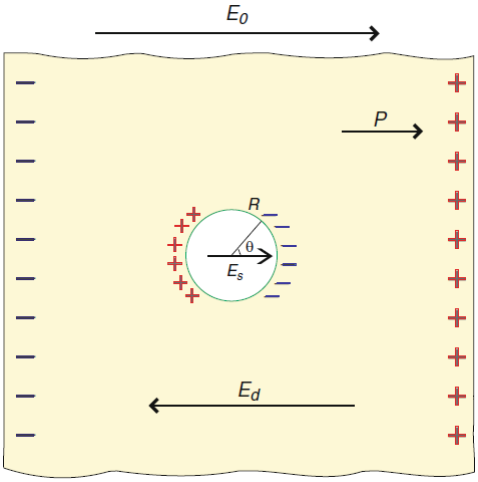

Figure 3.2: The Lorentz sphere concept for calculating the local field E_L. [5]

The macroscopic field is $E = E_0 + E_d$, and the contribution from local effects are considered in E_S. For calculating the microscopic effects we let α denote the polarizability of one molecule, so that the polarization density $\overrightarrow{P}$ is expressed as:

$$\overrightarrow{P} = N\alpha_i \overrightarrow{E_L} = N\alpha(\epsilon_h \overrightarrow{E} + \frac{L_i}{\epsilon_0 \epsilon_h} \cdot \overrightarrow{P}) \tag{3.2}$$

N- the NS concentration $[\frac{\#}{m^3}]$

[2]The most common notation in the literature is for $\epsilon_h = 1$. A transformation has been done for changing the medium permittivity $\epsilon_0 -> \epsilon_h \epsilon_0$

α_i−the polarizability in units of $[\frac{A^2 \cdot s^4}{kg}]$ in the i-axis. It is more intuitive to think in cgs where the units are $[cm^3]$

Another equation can be derived by considering the collective effect and the macroscopic electric field, $\overrightarrow{E}$. Equating the induced displacement inside the sphere from the effective field, E, and corresponding polarization (LHS), to the straight forward calculation of the displacement inside the sphere using the effective field in a medium with ϵ_r (RHS), gives:

$$\epsilon_0 \epsilon_h \overrightarrow{E} + \frac{\overrightarrow{P}}{\epsilon_h} = \epsilon_0 \epsilon_r \overrightarrow{E} \tag{3.3}$$

By rearrangment, the following equation is obtained:

$$\overrightarrow{P} = \epsilon_0 \epsilon_h (\epsilon_r - \epsilon_h) \overrightarrow{E} \tag{3.4}$$

where $\overrightarrow{P}$ stands for the polarization density. In a homogeneous media, $\epsilon_r = \epsilon_h$, and the polarization effect vanishes, which means that this will become a surface effect.

The outcome of equating the above two equation for $\overrightarrow{P}$, (3.2) and (3.4), is the effective (collective) polarizability :

$$\alpha_i = \frac{1}{N} \cdot \frac{\epsilon_0 \epsilon_h (\epsilon_r - \epsilon_h)}{\epsilon_h + L_i \cdot (\epsilon_r - \epsilon_h)} \tag{3.5}$$

which equals the Clausius-Mossetti relation for a spheroid ($L_i = \frac{1}{3}$) .
α_i depends on the next features of the system:

1. Wavelength due to ϵ_r (and ϵ_h)
2. NS geometry- due to L_i
3. Fraction of metal, f - due to $N = \frac{1}{V_{unit-cell}}$, where $V_{unit-cell}$ is the average volume for one NS. This factor only scales α_i and doesn't change the resonance behavior while f is low enough, as long as we work in the dipole approximation.

In the following, we add several clarifications about polarization, dipole-moment and polarizability:

1. Polarizability, α, is the ability to form instantaneous dipoles: $p = \alpha \cdot E$, where p is the dipole moment and E the electric field [8].

2. Electric dipole moment, p , a measure of the separation of positive and negative electrical charges within a system, that is, a measure of the system's overall polarity. The dipole moment density of the array, $p(r)$, contains both the location and the dipole moment [9].

3. Polarization density, $P(r)$, is the relevant value for calculation of Maxwell's equations [10].

A semi-classical model can be deduced by transforming from the microscopic methodology (α_i) to an effective macroscopic methodology (α_{eff}) by noting:

1. $[\alpha] = volume$ in cgs-units (can easily be seen by posting $\epsilon_0 = 1$).

2. The source of the polarizability is mostly the interface between the metal and the dielectric.

One can find the relation between the methodologies by $\alpha_{eff} = f\alpha_i$, where f is the filling volume density of the metal in the dielectric. The density of the polarizability for the metallic ellipsoid is:

$$fN\alpha_i = f\frac{\epsilon_0\epsilon_h(\epsilon_r - \epsilon_h)}{\epsilon_h + L_i \cdot (\epsilon_r - \epsilon_h)} \tag{3.6}$$

and the effective polarizability of the combination of the metal and the dielectric can be found by the transformation $\epsilon_r \to \epsilon_{eff}$ and $L_i \to L_{eff}$, where mostly the second transformation is not used:

$$N\alpha_{eff} = \frac{\epsilon_0\epsilon_h(\epsilon_{eff} - \epsilon_h)}{\epsilon_h + L_{eff} \cdot (\epsilon_{eff} - \epsilon_h)} \tag{3.7}$$

The left-hand side of the last two equations are equal. By equating the right-hand side of last two equation, one gets an expression for ϵ_{eff} :

$$\begin{aligned}\epsilon_{eff} &= \epsilon_h \cdot \frac{\epsilon_r(L_1 + f(1 - L_{eff})) + \epsilon_h(1 - L_1 - f(1 - L_{eff}))}{\epsilon_r(L_1 - L_{eff} \cdot f) + \epsilon_h(1 - L_1 + L_{eff} \cdot f)} = (L_1 = L_{eff}) = \\ &= \epsilon_h \cdot \frac{\epsilon_r(L_1(1 - f) + f) + \epsilon_h(1 - f)(1 - L_1)}{\epsilon_r L_1(1 - f) + \epsilon_h(1 - L_1(1 - f))}\end{aligned} \tag{3.8}$$

which can be a simplified to:

$$\begin{aligned}\epsilon_{eff} &= \epsilon_h + \epsilon_h \cdot f \cdot \frac{\epsilon_r - \epsilon_h}{\epsilon_r L_1(1-f) + \epsilon_h(1 - L_1(1-f))} \\ &= \epsilon_h + \epsilon_h \cdot f \cdot \frac{\epsilon_r - \epsilon_h}{\epsilon_h + (\epsilon_r - \epsilon_h) \cdot L_1(1-f)}\end{aligned} \tag{3.9}$$

For a sphere $L_1 = L_{eff} = \frac{1}{3}$, and the result is :

$$\epsilon_{eff} = \epsilon_h \frac{\epsilon_r(1+2f) + \epsilon_h(1-f)}{\epsilon_r(1-f) + \epsilon_h(2+f)} \tag{3.10}$$

as can be seen in [5] [11].

The cross-sections (in SI units) depend on the polarizability [4] [12] [13]:

$$C_{abs} = k \cdot Im(\alpha) \tag{3.11}$$

$$C_{scattering} = \frac{k^4|\alpha|^2}{6\pi} \tag{3.12}$$

$$C_{ext} = C_{abs} + C_{scattering} = k \cdot Im(\alpha) + \frac{k^4|\alpha|^2}{6\pi} \tag{3.13}$$

where C_{abs} stands for the electric-field energy absorbed by the plasmons while $C_{scattering}$ is the electric-field energy scattered from the NS.

When the NSs are much smaller than the wavelength of light (the "quasi-static" limit), the extinction cross section is dominated by the absorption ($C_{abs} \gg C_{scattering}$) [3] [14] [15] as can be shown from Mie-theory and consequently can be written as:

$$C_{ext} \approx C_{abs} = k \cdot Im(\alpha) \tag{3.14}$$

Generally, the absorption cross section for ellipsoid was developed by Gans:

$$C_{abs} = \frac{2\pi c}{3\lambda} \epsilon_m^{3/2} \sum_{j=1-3} \frac{(1/L_j^2)\epsilon_2}{(\epsilon_1 + \frac{(1-L_j)}{L_j}\epsilon_m)^2 + \epsilon_2^2} \tag{3.15}$$

where L_j is the depolarization factor in the j-axis and the metal permittivity equals

to $\epsilon_r = \epsilon_1 + i\epsilon_2$. The line-width of the LSPR can be calculated using [14]:

$$\Gamma_{eff} = \frac{2\epsilon_2}{|\frac{\partial\epsilon_1}{\partial\omega}|} \tag{3.16}$$

which can be derived using Taylor expansions of $\epsilon_1(\omega)$ and $\epsilon_2(\omega)$ near the resonance where $\epsilon_1 + \frac{(1-L_j)}{L_j}\epsilon_m \approx 0$, and by using $|\frac{\partial\epsilon_1}{\partial\omega}| \gg |\frac{\partial\epsilon_2}{\partial\omega}|$ as is known for noble metals.

The behavior of the resonance wavelength, λ_{LSPR}, of metallic ellipsoid with a small imaginary permittivity part ($\epsilon_1 \gg \epsilon_2$) in a dielectric medium [16] is described by:

$$\lambda_{LSPR} = \lambda_p \cdot \sqrt{\epsilon_1^{ib}(\lambda_{LSPR}) + \frac{1-L_i}{L_i} \cdot \epsilon_h} \tag{3.17}$$

where ϵ_1^{ib} is the real part of the the interband permittivity which can be neglected for longer wavelengths far from interband transition.

λ_{LSPR} is red shifted $\leftrightarrow$ $\frac{1-L_i}{L_i} \cdot \epsilon_h$ increases $\leftrightarrow$((ϵ_h increases) or (L_i decreases $\leftrightarrow$ the ellipsoid is longer)). This conclusion was verified using Comsol and is known in the literature. It is worth mentioning that in a cubic shape for example, the shape is 'longer' if we rotate it by 45^o where the diagonal is on the field axes, which in turns, redshifts the resonance.

3.1.3 Perturbative approach for calculation of thin layer influence on LSPR

Motivation

Our motivation for dealing with thin layers in plasmonic systems appeared while trying to match measurements of NS transmission spectrum, Comsol simulations and the MGT. The MGT treats a system with a metallic NS in an homogeneous dielectric medium while our fabrications are done with a metal over a thin Indium Tin Oxide (ITO) adhesion layer attached to a SiO_2 and on top of the NS there is air. It means that the original analytical MGT solution is for 2 materials while the fabrications have a minimum of 4 materials.

In this section we will concentrate on expanding MGT to match our fabrications which include ITO thin layer.

ITO and its optical properties

ITO is a ternary composition of indium, tin and oxygen in varying proportions. It is widely used in nano fabrications as a thin film adhesion layer between the Silica substrate and metal NS because of its two main properties: Its electrical conductivity and optical transparency, which mostly conflicts in nature. The conductivity and absorption in the infrared (IR) are influenced by the free carriers concentration. As the free carrier concentration increases, the absorption also increases and shifts toward shorter wavelengths [17]. In the nano fabrications, ITO is commonly deposited on surfaces by physical vapor deposition (PVD). Often used in electron beam evaporation, or a range of sputter deposition techniques [18].

ITO is a subject for research nowadays [19] [20]. It has a time and wavelength dependent refractive index with a significant imaginary part (absorptive) starting from wavelengths of about 1100nm (which is fabrication dependent). Our desired fabrication is a metallic (e.g Gold or Aluminum) NS over a dielectric (e.g Silica) surface. However, an intermediate layer must be used for sticking the two layers together using a metal oxide adhesion which improves the wetting strength (the ability of a liquid to maintain contact with a solid surface) of the metal-oxide interface. ITO can play the role of adhesion layer in our research cases because:

1. It attaches the metallic NS to the dielectric layer.
2. The ITO plays the role of conducting away the electrons when using an E-beam during the fabrication.
3. The EMT still works with some variations (as will be discussed later on)

Though the use of ITO in our fabrications is a necessity and adds unwanted complications to our models. The main complications with modeling the ITO with EMT in our cases are:

1. If the ITO layer it thin - a three layers EMT model needs to be used.
2. Its refractive index is wavelength dependent and its imaginary part becomes significant starting from wavelength of about 1100nm for regular ITOs.
3. Its optical properties varies between manufacturer and even from each 'bulk production series'.

To overcome the complications - a special ITO with negligible imaginary part up to 2 microns was manufactured for our experiments and its spectroscopy values were measured.

We have also developed a theoretical model, which expands the current theory and includes the effects of a thin layer on LSPR. This is described in the following sections.

Perturbative approach theory

For modeling the thin-layer (in our case ITO) effect on a LSPR our starting point was models from the literature. A change in the thickness of a layer has been shown to affect the LSPR only up to a height of 40% of the NS height [21] or for an other case up to 20nm [22] which means that for wider thin-layers of ITO the glass effect on the LSPR could be neglected. Consequently, 'thin layer's' height is $\lesssim 20nm$ in our fabrications.

In the literature [21] [23] [24] [25] this complication is mentioned and exploited. It was analytically solved by considering the thin layer as a perturbation in the material properties [26]:

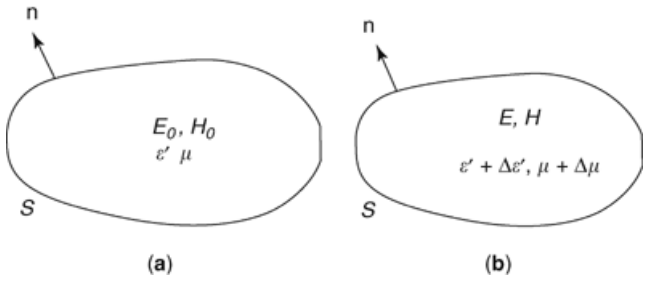

Figure 3.3: Perturbative approach for thin layers. The theortical model was adapted from [26]

The complete physical derivation of the perturbation theory is based on perturbations in the Maxwell's electromagnetic equations assuming small shift of the resonance: $\frac{\omega-\omega_0}{\omega_0} \approx \frac{\omega-\omega_0}{\omega}$ [27]. The main result is:

$$\frac{\omega-\omega_0}{\omega_0} \approx -\frac{\int\int\int \Delta\epsilon \cdot E_{int} \cdot E_0^* d\tau}{2 \cdot \int\int\int \epsilon |E_0|^2 d\tau} \tag{3.18}$$

where, ω is the new resonance, ω_0 is the resonance of the original cavity, $d\tau$ is for the integration over the volume of the cavity, ϵ is the original permittivity, E_0 is the electric field of the original cavity and E_{int} stands for the electric field after the perturbation. In our case $\Delta\epsilon \neq 0$ only where the adhesion layer was added and by assuming that the electric-field doesn't change much because the adhesion layer is thin ($E_{int} \approx E_0$) , we obtain:

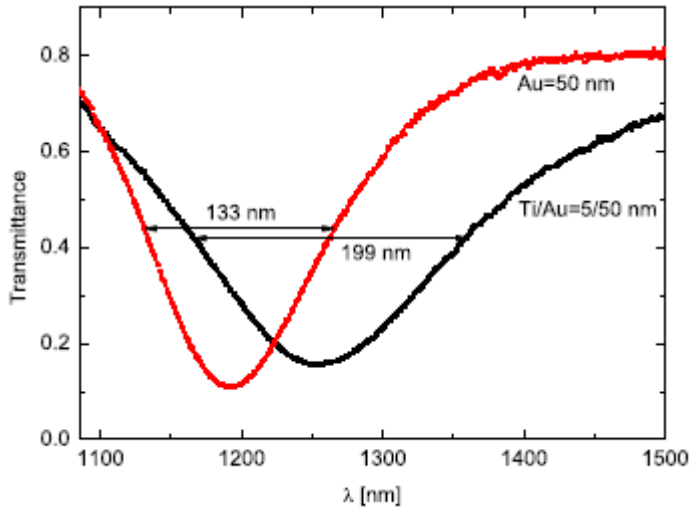

Figure 3.4: Transmission spectra for samples with and without a 5 nm Ti adhesion layer measured at normal incidence [23]

$$\frac{\omega - \omega_0}{\omega_0} \approx -\frac{f}{2} \cdot \frac{\epsilon_{adh} - \epsilon_{silica}}{\epsilon_{silica}} \tag{3.19}$$

where f is the fraction of adhesion layer volume from the total volume and the ω shift (real and imaginary parts) has a linear dependency with small f.

Assuming $Im\{\epsilon_{silica}\} = 0$ and $Im\{\omega_0\} = 0$, by substituting $\omega = \omega' + i\omega''$ and $\epsilon_{adh} = \epsilon_{edh}^{'} + i\epsilon_{adh}^{''}$ one can derive the resonance shift [23]:

$$\frac{\Delta\omega}{\omega_0} \approx -\frac{f}{2} \cdot \frac{\epsilon_{adh} - \epsilon_{silica}}{\epsilon_{silica}} \tag{3.20}$$

By using $\omega^{''} = \omega^{''} - Im\{\omega_0\} = \Delta\omega^{''} = \Delta\Gamma$, where $\Delta\Gamma$ stands for the resonance broadening:

$$\frac{\Delta\Gamma}{\omega_0} \approx -\frac{f}{2} \cdot \frac{\epsilon_{adh}^{''}}{\epsilon_{silica}} \tag{3.21}$$

The theoretical results were verified by measurements in the article, as can be seen in Figure 3.4.

The dependency between the broadening and the resonance shift is:

$$\Delta\Gamma = \chi \cdot \Delta\omega, \chi = \frac{\epsilon''_{adh}}{\epsilon'_{adh} - \epsilon_{silica}} \tag{3.22}$$

In the article they got $\chi_{measured} \sim 2 \cdot \chi_{theory}$ because they measured $2 \cdot \Delta\Gamma$ and by setting the right value of $\Delta\Gamma$, the experimental results improve significantly.

The problem is still that the exact properties of the ITO layer are usually not known with good accuracy. Practically, the ITO induces resonances' shift which can be found by comparing $\lambda_{res}^{measured}$ to λ_{res}^{theory}.

There are still some basic not fulfilled assumptions in the theory:

1. f: Not defined well because it should take care of all the volume which takes part in the interaction and not just the NS- We will address this problem later.

2. The medium is just a 'bulk medium': unlike the theory that takes into account a uniform medium surrounding the nanoparticles, in reality the nanoparticles' surrounding medium is both glass and air. We address this problem later.

3. $\frac{\omega-\omega_0}{\omega_0} \approx \frac{\omega-\omega_0}{\omega}$: This assumption is mostly not true and should not be made - Solved later.

4. No exponential decay of the fields in the effective volume (although it is mentioned in the literature [22]: This assumption can be possibly dealt with by employing more sophisticated approaches.

5. No significant changes in the electric fields: Will stay as an assumption, otherwise the above simplified equation [3.19] could not be done.

A new model that I have developed dealing with [1-3] assumptions, will be introduced in part 6.3.

3.2 Femtosecond-scale phenomenon

Femtosecond (fs) scale phenomena are non-intuitive at first glance to the common researcher. In order to explore such ultrafast phenomena, a fs-laser is used, meaning that our time-resolution is of 'fs-scale'. Moreover, a fs-laser emits concentrated power in a short pulse which enables us to examine non-linear effects.

This chapter mostly concentrates on phenomena related to the 3rd order nonlinear susceptibility, $\chi^{(3)}$, where the EM-wave affects itself. An example of such effect is the

change in the plasmon's extinction cross-section ($\frac{\partial\sigma_{ext}(\lambda,t)}{\partial t}$) due to temperature changes of the lattice and electrons caused by the preceding part of the absorbed EM pulse. In Ref. [28], R. Boyd, explored the third order non-linearity. He showed that the $\chi^{(3)}$ calculated and measured in different articles were different in orders of magnitude, where $\chi^{(3)}$ is defined in the optical nonlinear equation $P(t) = \sum \chi^{(i)} E^i(t)$. In order to achieve consistent results, one should understand the $\chi^{(3)}$ phenomena measured.

3.2.1 Time dependent extinction cross-section

As seen above, the plasmon's cross section depends on the materials of the NS and the medium. As we will show later, the TTM predicts time-dependent dynamics in the electrons and lattice temperatures, $T_e(t)$ and $T_l(t)$ respectively. These dynamics result in changes in the dielectric function $\epsilon = \epsilon_1 + i\epsilon_2$. Consequently, the LSPR red-shifts and broadens.

The phenomenon can be observed in a pump-probe experiment, as can be seen in Fig. [3.5], where the blue (red)-detuned EM pulse is absorbed less (more) than the resonance during time, respectively [29]. The phenomena is modeled for small changes assuming a first order expansion:

$$\Delta\sigma_{ext}(\lambda,t) = \frac{\partial\sigma_{ext}}{\partial\epsilon_1}(\lambda)\cdot\Delta\epsilon_1(\lambda,t) + \frac{\partial\sigma_{ext}}{\partial\epsilon_2}(\lambda)\cdot\Delta\epsilon_2(\lambda,t) \tag{3.23}$$

where $\frac{\partial\sigma_{ext}}{\partial\epsilon_i}(\lambda)$ depends on the cross-section of the NS as shown in the above chapters. $\Delta\epsilon_i(\lambda,t)$ ($i \subseteq \{1,2\}$) are the metal's real and imaginary permittivities which depend on the temperatures of the electrons, T_e, and lattice, T_l. As will be seen in the next chapter, T_e and T_l are time dependent.

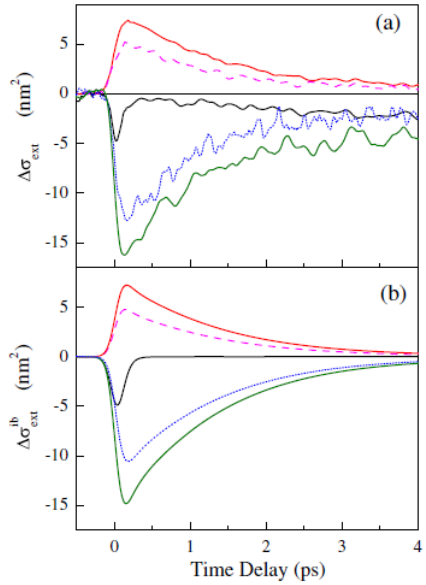

Figure 3.5: (a) Time-dependent $\Delta\sigma_{ext}(\lambda_{pr}, t_D)$ measured for the Au nanorod of at different probe wavelengths λ_{pr} around its LSPR: from top to bottom $\lambda_{pr} - \lambda_R \approx +30, +40, 0, -30, and -20nm$ ($\lambda_R \approx 810nm$) (b) Computed interband contribution $\Delta\sigma^{ib}_{ext}(\lambda_{pr}, t_D)$ for the same λ_{pr}. The excitation corresponds to $\Delta T_e^{max} = 125K$ [29]

3.2.2 Two temperature model

The Two Temperature Model (TTM) comes to explain the general light-matter interaction in the fs-ps time-scale and is an outcome from of Boltzmann equation. The interaction can be divided into steps:

1. Photons interact with electrons through interband and intraband interaction, which consequently takes electrons out of Fermi-Dirac distribution. Those electrons are called 'Non-Thermalized Electrons' (NTE).

2. The NTE pass their energy to the thermalized electrons and lattice through scattering. T_e climbs to a much higher temperature than T_l. The thermalized electrons are called "hot electrons" as long as they have well defined Fermi-Dirac distribution and their temperature is higher than the temperature of the lattice.

3. The "hot electron" exist until T_e and T_l equilibrate through electron-lattice scattering.

In our fs-nm regime, the TTM must take into account the NS effects. The interaction steps are very similar, but have some effects, which outcome from the NS as can be seen in Fig [3.6]. The EM pulse can be absorbed also through the LSPR which is time (temperature) dependent, as we have discussed above. Moreover, the phonons absorbed

energy translates into an acoustic wave, causing to the oscillations in the physical size of the NS (breathing mode). During these processes, energy diffuses to the environment. A more thorough explanation of the process can be seen in [1] [14] [16].

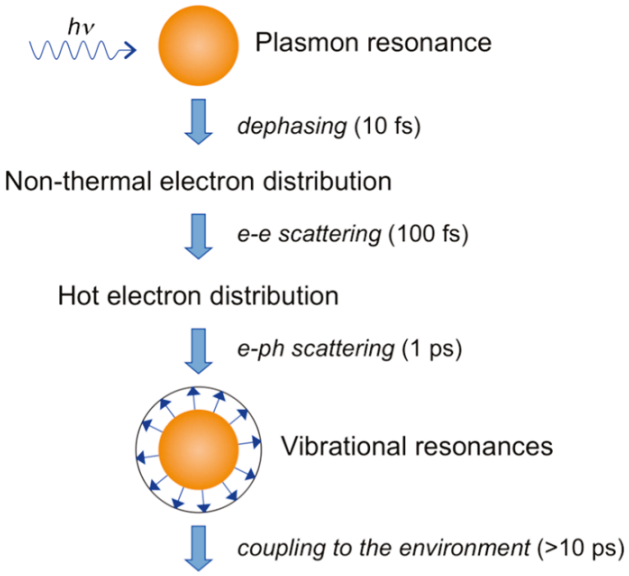

Figure 3.6: Sequence of events and approximate time scales following absorption of photons by a metal nanoparticle [14]

Our research will concentrate on the time scale of fs up to a few ps. Consequently, the vibrational resonances and the spatial energy diffusion to the environment will be ignored for simplicity.

One should note that the TTM have some variations which emphasize phenomena in different materials, sizes and time scales. For an accurate model describing the interaction on a fs-ps time scale, one can check the TTM introducing a nonthermal lattice model for describing nonthermal phonon distributions which origin from longitudinal acoustic phonons [30].

The coupled-equations describing the TTM, gives a good glance into the fs-ps time scale interaction [31]:

$$\begin{aligned} \partial_t N(t) &= -(\gamma_e + \gamma_l)N(t) + P_A(t) \\ C_e(t) \cdot \partial_t T_e(t) &= -G(T_e - T_l) + \gamma_e N(t) \\ C_l(t) \cdot \partial_t T_l(t) &= G(T_e - T_l) + \gamma_l N(t) \end{aligned} \tag{3.24}$$

where, $N(t)$ is the NTE's energy. γ_e, γ_l $(\frac{1}{\tau})$ are the electron-electron (e-e) and electron-phonon (e-ph) scattering parameters, respectively. $P_A(t)$ is the absorbed power, T_e and

T_l are the electrons and lattice temperatures. C_e and C_l are the heat capacities of the electrons and lattice ($C_e \ll C_l$), and G is the coupling between the electrons and the lattice.

The equations resemble energy transfer between 3 main players- NTEs, thermalized electrons and the lattice. There are some hidden approximations and assumptions in the equations:

1. The use of temperatures is non trivial because the TTM deals with non-equilibrium system. On the other hand, it is assumed that each subsystem (electrons, lattice) is in equilibrium [32], i.e. one can assign a Fermi-Dirac distribution to each of them separately.

2. $C_e(T_e(t)), C_l(T_l(t)), G(T_e(t))$- are time dependent. Consequently, the equations should have been such that the energy change of the electrons and lattice expressed as $\partial_t(C_e(t) \cdot T_e(t))$ and $\partial_t(C_l(t) \cdot T_l(t))$, but in the literature, in most of the experimental paper, the equations are not represented in such a way except for a theoretical paper [33].

3. Small size effects of γ_e and γ_l can be ignored in our NS because the length of the NS is above of the mean free path length in gold, i.e. $r > 20nm$ [14].

4 Exploring ultrafast phenomena

4.1 Motivation

Ultrafast phenomena in plasmonic nanostructures was extensively studied in ths last few years. We demonstrate that temporal manipulation of an incoming ultrafast pulse affects the spatio-temporal-spectral plasmonic system.

As mentioned in chapter [2], we study the photo-induced ultrafast dynamics in plasmonic nanostructures which show that at the femtosecond time scale, the electrons and the lattice of the the plasmonic system have different temperatures after an interaction with an incoming pulse. The phenomena were not yet explored via coherent control methods as shown later. Coherent control can be achieved through pulse-shaping that is obtained by tailoring the spectral phases of the excitation pulse. For exploring the ultrafast phenomena, tools such as FROG and pulse-shapers are used. This will be detailed in the next sections [4.2].

4.2 Experimental apparatus

4.2.1 Introduction

In order to characterize a fs pulse, which is much faster than any electronic-based measurement devices, one should use the pulse itself for the measurement process. In the past two decades, several characterization techniques have developed. Here, we use a custom built FROG (Frequency-Resolved Optical Gating) for measuring pulse's amplitudes and phases. Moreover, a number of spectrometers for different wavelengths range and sensitivity must be used for exploring nonlinearity of wave mixing (e.g DFG, SFG, THG, SHG and FWM).

For manipulating the amplitude and phase of a laser pulse, a pulse-shaper configuration was built with an SLM in its Fourier plane, as will be discussed later.

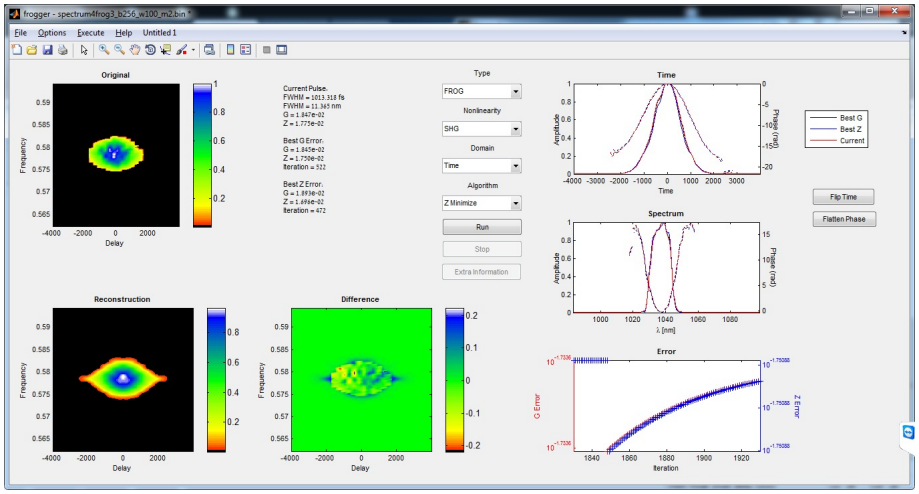

Figure 4.1: The displayed screen of the FROG's pulse reconstruction. Top left is the measured SFG as a function of delay between the 2 beams. Bottom left is the SFG calculation of the reconstructed pulse. Right side plots, from top to bottom, are the reconstructed pulse in time domain, frequency domain and the error of the reconstruction.

Examples of controlling the phase through the pulse-shaper will be shown later on in my research.

4.2.2 Pulse-shaping

Introduction

Coherent control of ultrafast phenomena can be made using a pulse-shaper which manipulates the waveform of optical pulses. A pulse-shaper is built by placing a spatial light modulator (SLM) in a Fourier plane which can change the amplitude and phase of each wavelength separately. By changing each wavelength separately, the pulse in the time domain changes correspondingly and can be calculated using Fourier-Transform. A grating with 200 grooves/mm and a cylindrical-mirror with focal-length of 456.7mm is being used with the SLM-S640d JENOPTIK in the pulse-shaper.

More information on the standard pulse-shaper configuration can be found in references [34] [35].

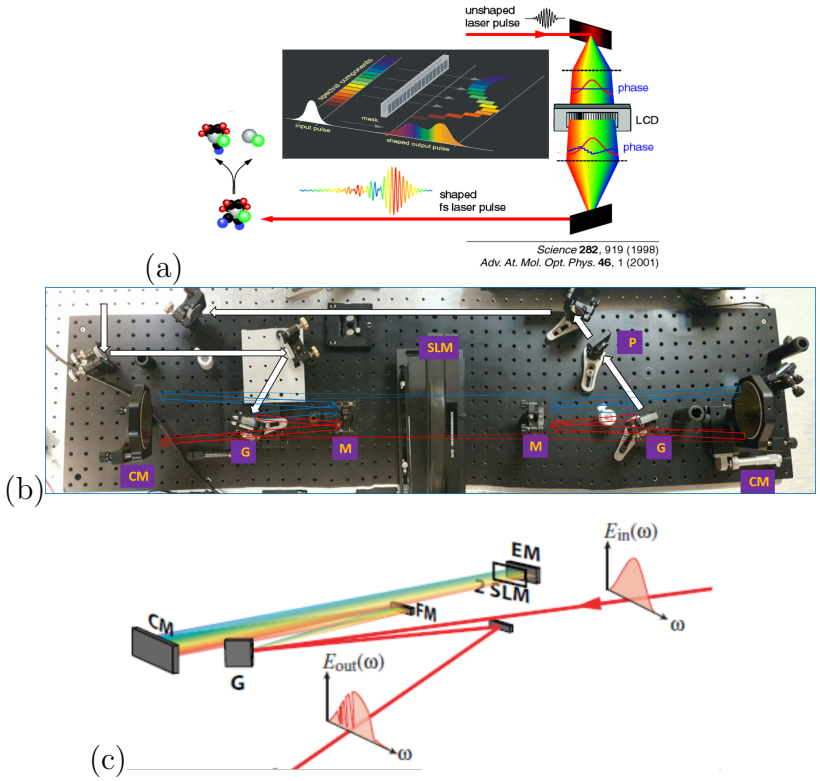

Figure 4.2: (a) A pulse-shaper configuration. The spectral phase of the pulse is shaped in the Fourier-plane by an LCD/SLM, thus the temporal shape. (b) Picture of the pulse-shaper in the laboratory. Blue represent the shorter wavelengths and red the long ones. G=Grating, M=Mirror, CM=Cylindrical-Mirror, P=Polarizer. SLM= SLM-S640d JENOPTIK (c) Folded pulse-shaper configuration.

Pulse-shaper - Folded configuration

The standard pulse-shaper configuration is symmetric compared to the Fourier plane where the SLM is placed. For making the pulse-shaper half in size and components using a folded-configuration, a mirror can be attached right after the SLM so that the pulse will walk back almost at the same path it came from, as can be seen is Fig [4.2c].

The SLM-S640d JENOPTIK [35] is formed by two precisely coupled liquid crystal (LC) masks. Each cell can be controlled separately. The LC is a nonlinear (NL) medium which have refractive indexes of n_o and n_e which correspond to the crystals axes. The crystal's orientation can be controlled by changing a voltage over each cell separately.

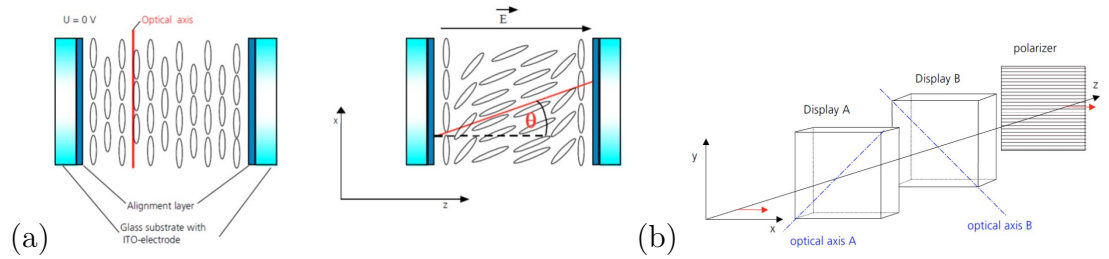

Figure 4.3: (a) LC orientation in an electrical field. For light traveling in z-direction (perpendicular to the glass substrates), birefringence takes place, resulting in two linearly polarized partial beams (one polarized in x-direction and one in y-direction). (b) Coupling of two LC cells for independent modulation of amplitude and phase of a linearly polarized incident light wave.

For light propagating in the z-direction, the refractive index of the field in the y-polarization is $n_y = n_o$ while the effective refractive index in the x-polarization is calculated as a birefringent material where $\theta(U)$ is voltage dependent:

$$\frac{1}{n_x^2(\theta(U))} = \frac{cos^2(\theta(U))}{n_o^2} + \frac{sin^2(\theta(U))}{n_e^2} \tag{4.1}$$

A change in the polarization is caused by a phase difference ϕ between ordinary and extraordinary rays and is calculated for wavelength λ_0 from:

$$\Delta\phi = \phi_e - \phi_o = 2\pi \cdot (n_x(U) - n_y) \cdot \frac{d_{LC}}{\lambda_0} = \frac{\omega}{c} \cdot \Delta n(U) \cdot d_{LC} \tag{4.2}$$

where d_{LC} is the propagation length of the light in the LC.

The SLM manipulated a linear-polarized light by changing its polarization twice with two different masks for each wavelength so that two parameters of the light can be controlled, the amplitude and phase. The manipulation on the polarized light can be described mathematically using Jones formalism. In our case the optical axis (OA) of 'Display A' have an angle of $\varphi_1 = 45^o$ in respect to the x-axis and 'Display B' have $\varphi_2 = -(90 - \varphi_1) = -45^o$.

The outgoing wave after the polarizer is calculated by:

$$\overrightarrow{\epsilon_{out}} = \overbrace{\begin{bmatrix} 1 & 0 \\ 0 & 0 \end{bmatrix}}^{polarizer} \cdot \overbrace{\begin{bmatrix} cos(-\varphi_2) & sin(-\varphi_2) \\ -sin(-\varphi_2) & cos(-\varphi_2) \end{bmatrix} \cdot \begin{bmatrix} 1 & 0 \\ 0 & e^{i\Delta\phi_2} \end{bmatrix} \cdot \begin{bmatrix} cos(\varphi_2) & sin(\varphi_2) \\ -sin(\varphi_2) & cos(\varphi_2) \end{bmatrix}}^{LC\ cell\ with\ phase\ retardation\ \Delta\phi_2} \cdot \tag{4.3}$$

$$\cdot \overbrace{\begin{bmatrix} cos(-\varphi_1) & sin(-\varphi_1) \\ -sin(-\varphi_1) & cos(-\varphi_1) \end{bmatrix} \cdot \begin{bmatrix} 1 & 0 \\ 0 & e^{i\Delta\phi_1} \end{bmatrix} \cdot \begin{bmatrix} cos(\varphi_1) & sin(\varphi_1) \\ -sin(\varphi_1) & cos(\varphi_1) \end{bmatrix}}^{LC\ cell\ with\ phase\ retardation\ \Delta\phi_1} \cdot \overrightarrow{\epsilon_{in}}$$

where for $\varphi_1 = 45^o$ and $\varphi_2 = -45^o$:

$$\begin{bmatrix} cos(-\varphi_1) & sin(-\varphi_1) \\ -sin(-\varphi_1) & cos(-\varphi_1) \end{bmatrix} \cdot \begin{bmatrix} 1 & 0 \\ 0 & e^{i\Delta\phi_1} \end{bmatrix} \cdot \begin{bmatrix} cos(\varphi_1) & sin(\varphi_1) \\ -sin(\varphi_1) & cos(\varphi_1) \end{bmatrix} = \tag{4.4}$$

$$= exp[i\frac{\Delta\phi_1}{2}] \cdot \begin{bmatrix} cos(\frac{\Delta\phi_1}{2}) & -i \cdot sin(\frac{\Delta\phi_1}{2}) \\ -i \cdot sin(\frac{\Delta\phi_1}{2}) & cos(\frac{\Delta\phi_1}{2}) \end{bmatrix} =$$

$$= exp[i\frac{\Delta\phi_1}{2}] \cdot \overleftrightarrow{\mu}(\frac{\Delta\phi_1}{2})$$

$$\begin{bmatrix} cos(-\varphi_2) & sin(-\varphi_2) \\ -sin(-\varphi_2) & cos(-\varphi_2) \end{bmatrix} \cdot \begin{bmatrix} 1 & 0 \\ 0 & e^{i\Delta\phi_2} \end{bmatrix} \cdot \begin{bmatrix} cos(\varphi_2) & sin(\varphi_2) \\ -sin(\varphi_2) & cos(\varphi_2) \end{bmatrix} = \tag{4.5}$$

$$= exp[i\frac{\Delta\phi_2}{2}] \cdot \begin{bmatrix} cos(-\frac{\Delta\phi_2}{2}) & i \cdot sin(-\frac{\Delta\phi_2}{2}) \\ i \cdot sin(-\frac{\Delta\phi_2}{2}) & cos(-\frac{\Delta\phi_2}{2}) \end{bmatrix} =$$

$$= exp[i\frac{\Delta\phi_2}{2}] \cdot \begin{bmatrix} cos(\frac{\Delta\phi_2}{2}) & -i \cdot sin(\frac{\Delta\phi_2}{2}) \\ -i \cdot sin(\frac{\Delta\phi_2}{2}) & cos(\frac{\Delta\phi_2}{2}) \end{bmatrix} = \tag{4.6}$$

$$= exp[i\frac{\Delta\phi_2}{2}] \cdot \overleftrightarrow{\mu}(-\frac{\Delta\phi_2}{2})$$

where we defined $\overleftrightarrow{\mu}(\theta) = \begin{bmatrix} cos(\theta) & -isin(\theta) \\ -isin(\theta) & cos(\theta) \end{bmatrix}$ and $\overleftrightarrow{\mu}(\theta_1) \cdot \overleftrightarrow{\mu}(\theta_2) = \overleftrightarrow{\mu}(\theta_1 + \theta_2)$.
The final result can be easily calculated:

$$\overrightarrow{\epsilon_{in}} = \begin{bmatrix} 1 \\ 0 \end{bmatrix} \cdot E_0 e^{i(\omega t - kx)} \tag{4.7}$$

$$\overrightarrow{\epsilon_{out}} = \overrightarrow{\epsilon_{in}} \cdot cos(\frac{\Delta\phi_1 - \Delta\phi_2}{2}) \cdot e^{i(\frac{\Delta\phi_1+\Delta\phi_2}{2})} \tag{4.8}$$

The phase retardation of the first and second LC display (display A and B) acts on the 'Amplitude Modulation' A and on the 'Phase Modulation' ϕ as fallows:

$$A = cos(\frac{\Delta\phi_1 - \Delta\phi_2}{2}) \tag{4.9}$$

$$\phi = \frac{\Delta\phi_1 + \Delta\phi_2}{2} \tag{4.10}$$

In a folded configuration, a mirror is entered right after the SLM:

$$\begin{aligned}\overrightarrow{\epsilon_{out}} = {} & \overbrace{\begin{bmatrix} 1 & 0 \\ 0 & 0 \end{bmatrix}}^{polarizer} \cdot \overbrace{\begin{bmatrix} cos(-\varphi_1) & sin(-\varphi_1) \\ -sin(-\varphi_1) & cos(-\varphi_1) \end{bmatrix} \cdot \begin{bmatrix} 1 & 0 \\ 0 & e^{i\Delta\phi_1} \end{bmatrix} \cdot \begin{bmatrix} cos(\varphi_1) & sin(\varphi_1) \\ -sin(\varphi_1) & cos(\varphi_1) \end{bmatrix}}^{LC\ cell\ with\ phase\ retardation\ \Delta\phi_1} \cdot \\ & \cdot \overbrace{\begin{bmatrix} cos(\varphi_2) & sin(\varphi_2) \\ -sin(\varphi_2) & cos(\varphi_2) \end{bmatrix} \cdot \begin{bmatrix} 1 & 0 \\ 0 & e^{i\Delta\phi_2} \end{bmatrix} \cdot \begin{bmatrix} cos(-\varphi_2) & sin(-\varphi_2) \\ -sin(-\varphi_2) & cos(-\varphi_2) \end{bmatrix}}^{LC\ cell\ with\ phase\ retardation\ \Delta\phi_2} \cdot \overbrace{\begin{bmatrix} 1 & 0 \\ 0 & -1 \end{bmatrix}}^{mirror} \cdot \\ & \cdot \overbrace{\begin{bmatrix} cos(\varphi_2) & sin(\varphi_2) \\ -sin(\varphi_2) & cos(\varphi_2) \end{bmatrix} \cdot \begin{bmatrix} 1 & 0 \\ 0 & e^{i\Delta\phi_2} \end{bmatrix} \cdot \begin{bmatrix} cos(-\varphi_2) & sin(-\varphi_2) \\ -sin(-\varphi_2) & cos(-\varphi_2) \end{bmatrix}}^{LC\ cell\ with\ phase\ retardation\ \Delta\phi_2} \cdot \\ & \cdot \overbrace{\begin{bmatrix} cos(-\varphi_1) & sin(-\varphi_1) \\ -sin(-\varphi_1) & cos(-\varphi_1) \end{bmatrix} \cdot \begin{bmatrix} 1 & 0 \\ 0 & e^{i\Delta\phi_1} \end{bmatrix} \cdot \begin{bmatrix} cos(\varphi_1) & sin(\varphi_1) \\ -sin(\varphi_1) & cos(\varphi_1) \end{bmatrix}}^{LC\ cell\ with\ phase\ retardation\ \Delta\phi_1} \cdot \overrightarrow{\epsilon_{in}}\end{aligned} \tag{4.11}$$

And in the same way the amplitude and phase are easily found:

$$A = cos(\Delta\phi_1 - \Delta\phi_2) \tag{4.12}$$

$$\phi = \Delta\phi_1 + \Delta\phi_2 \tag{4.13}$$

The results were verified with the literature [36] and were checked in the laboratory.

4.2.3 Pulse-shaper - Experimental results

Amplitude-calibration verification: Blocking window

After the calibration processes of the SLM in a chosen pulse-shaper configuration, a performance check was done by giving a command to the SLM to block specific wavelengths range as can be seen in figure [4.4].

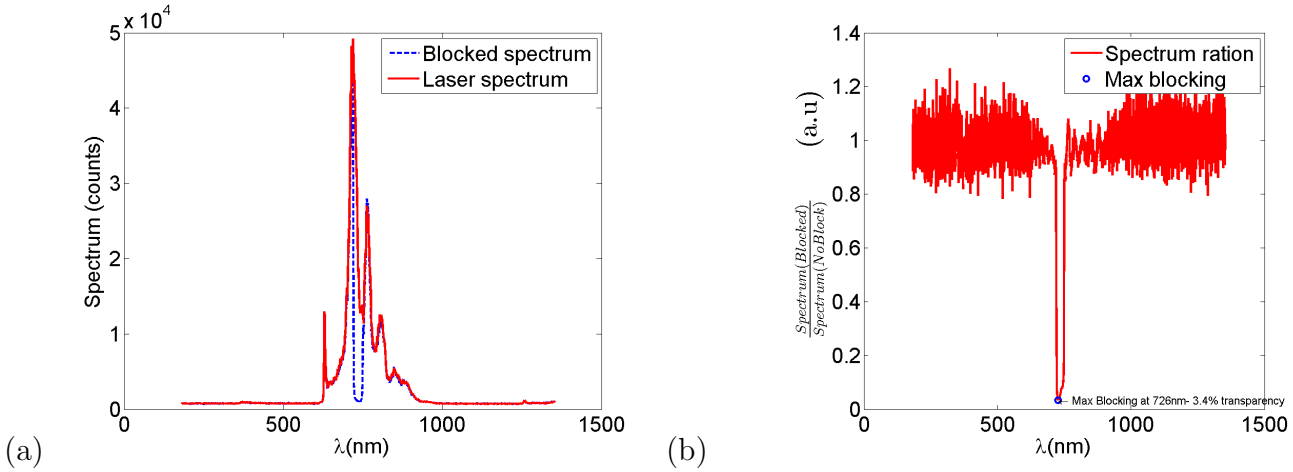

Figure 4.4: (a) Spectrum of laser with and without a blocking window in the SLM in a wavelengths range of 720-750nm (b) Transparency calculation- Ratio between with and without blocked spectrum at 720-750nm

Transform-limited calibration - SHG in instantaneous interaction material

A pulse accumulates quadratic phase while propagating in the free-space. A calibration must be done for compensating the accumulated phase for bringing the pulse as transform-limited to the target. Consequently, an opposite quadratic phase was added by shifting the pulse-shaper's gratings [37] and afterwards a fine tuning with the SLM was done by running many quadratic phases for finding the maximum SHG in a BBO crystal, as can be seen in Fig. [4.5].

Phase-calibration verification: Using coherent-control of SHG in instantaneous interaction material

After calibrating the pulse to be transform limited at the BBO, the SLM phase modulation was checked using coherent control techniques. The SHG is manipulated using techniques from atomic-physics such as Two Photon Absorption (TPA) [38]. The equations in the atomic physics case and in the SHG case are similar.

In the following, we will describe the interaction of EM field with atomic media in the nonresonant TPA regime. Consider a resonant interaction of a weak ultrashort pulse with

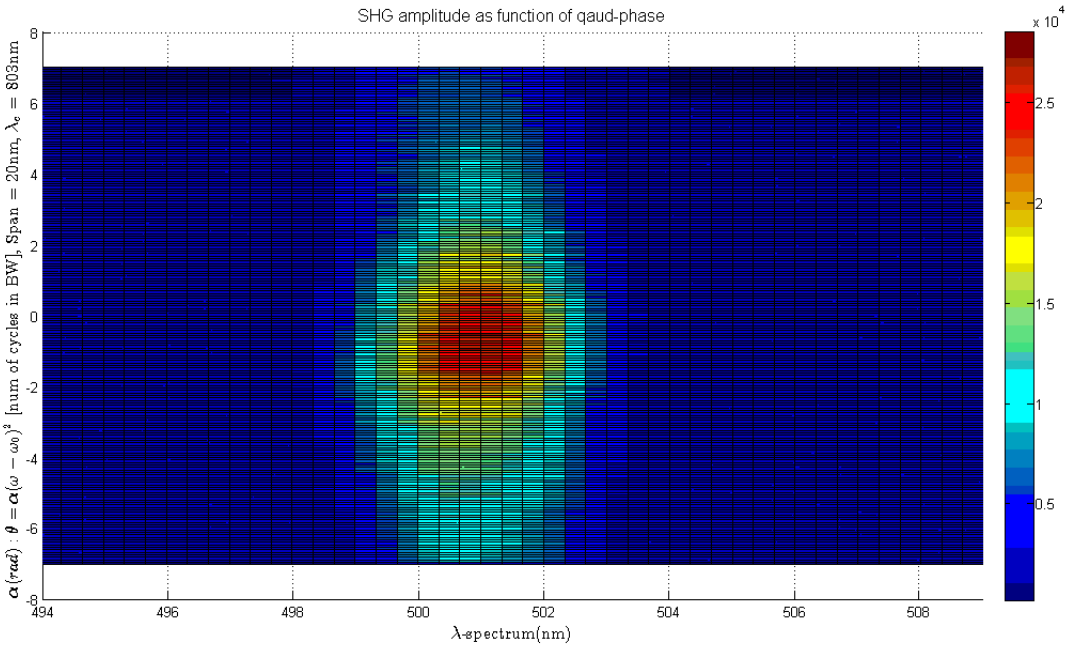

Figure 4.5: SHG spectrum intensity as function of quadratic phase for fine tuning the accumulated quadratic phase in the free space

a two-level atom where $|g\rangle$ and $|f\rangle$ are the ground and excited states, respectively. The electric field of the exciting pulse is $\epsilon(t)$ $(= V_I(t))$ and assumed to be much shorter than the lifetime of the excited state. In the interaction representation, the time-dependent potential is:

$$i\hbar\partial_t U_I(t, t_0) = V_I(t)U_I(t, t_0) \tag{4.14}$$

From second order non-resonant time-dependent perturbation theory, the amplitude of the excited state from TPA is:

$$a_f(t) \approx -\frac{1}{\hbar^2}\sum_n \mu_{fn}\mu_{ng}\int_{-\infty}^{t}\int_{-\infty}^{t_1}\epsilon(t_1)\epsilon(t_2)\cdot exp(i\omega_{fn}t_1)\cdot exp(i\omega_{ng}t_2)dt_2dt_1 \tag{4.15}$$

where n is an intermediate state, $\omega_{ij} = \frac{E_i - E_j}{\hbar}$ and μ_{ij} is the dipole moment matrix element. The summation is performed over all possible intermediate states of the unperturbed atom. Since we assume they are all far from resonance, the contribution of all intermediate levels will add coherently only for a very short duration ($t_1 \approx t_2$). After

some mathematical derivations:

$$S_2 = |\int_{-\infty}^{\infty} \epsilon^2(t) \cdot exp(i\omega_0 t)|^2 \tag{4.16}$$

where $\omega_0 = \frac{E_f - E_g}{\hbar}$. Using F.T theory where multiplication transforms to convolution:

$$\begin{gathered} |\int_{-\infty}^{\infty} \epsilon^2(t) \cdot exp(i\omega_0 t)dt|^2 = \\ = |\int_{-\infty}^{\infty} \tilde{\epsilon}(\Omega)\tilde{\epsilon}(\omega_0 - \Omega)d\Omega|^2 = (\Omega \to \Omega + \tfrac{\omega_0}{2}) = \\ = |\int_{-\infty}^{\infty} \tilde{\epsilon}(\tfrac{\omega_0}{2} + \Omega)\tilde{\epsilon}(\tfrac{\omega_0}{2} - \Omega)d\Omega|^2 = \\ = |\int_{-\infty}^{\infty} A(\tfrac{\omega_0}{2} + \Omega) \cdot A(\tfrac{\omega_0}{2} - \Omega) \cdot exp[i\{\Phi(\tfrac{\omega_0}{2} + \Omega) + \Phi(\tfrac{\omega_0}{2} - \Omega)\}]d\Omega|^2 \end{gathered} \tag{4.17}$$

where $\tilde{\epsilon}(\omega) = A(\omega) \cdot exp[\Phi(\omega)]$ is the F.T of $\epsilon(t)$ and $A(\omega)$ and $\Phi(\omega)$ are the spectral amplitude and spectral phase, respectively. The equation reflects that the two-photon transition occurs for all pairs of photons with frequencies which adds to ω_0 and lay within the spectrum of the exciting pulse. It is easily seen that cancellation of the spectral phase (i.e $\Phi(\frac{\omega_0}{2} + \Omega) + \Phi(\frac{\omega_0}{2} - \Omega) = 0$) results in maximization of the probability amplitude. This occurs for a transform-limited pulse ($\Phi(\Omega) = 0$) and for every anti-symmetric phase compared to $\frac{\omega_0}{2}$. The anti-symmetric phase can significantly affect the shape of the pulse to have much smaller amplitude and a much longer duration without affecting the TPA (as long as the pulse does not exceed the lifetime of the excited state) [38, 39].

Using the anti-symmetric phase technique the phase calibration can be verified. A π-step is inserted each time at a different wavelength and a SHG (or more precisely, Sum Frequency Generation, SFG) spectrum is measured. A destructive interference will appear in the SHG when the step is not in the middle of the spectrum ($\frac{\omega_0}{2}$), and could even go down to zero for a shift from the resonance, Ω_{step} , that fits the next equation:

$$For: \ \omega_{step} = \tfrac{\omega_0}{2} + \Omega_{step}, \ \Omega_{step} > 0$$

$$\begin{gathered} 0 = |\int_{\Omega_{step}}^{\infty} A(\tfrac{\omega_0}{2} + \Omega) \cdot A(\tfrac{\omega_0}{2} - \Omega)d\Omega + \int_0^{\Omega_{step}} A(\tfrac{\omega_0}{2} + \Omega) \cdot A(\tfrac{\omega_0}{2} - \Omega) \cdot exp[i\pi]d\Omega|^2 = \\ |\int_{\Omega_{step}}^{\infty} A(\tfrac{\omega_0}{2} + \Omega) \cdot A(\tfrac{\omega_0}{2} - \Omega)d\Omega - \int_0^{\Omega_{step}} A(\tfrac{\omega_0}{2} + \Omega) \cdot A(\tfrac{\omega_0}{2} - \Omega)d\Omega|^2 \end{gathered} \tag{4.18}$$

where the calculation can be generalized easily to any anti-symmetric phase. Measurement results can be seen in Figure [4.6].

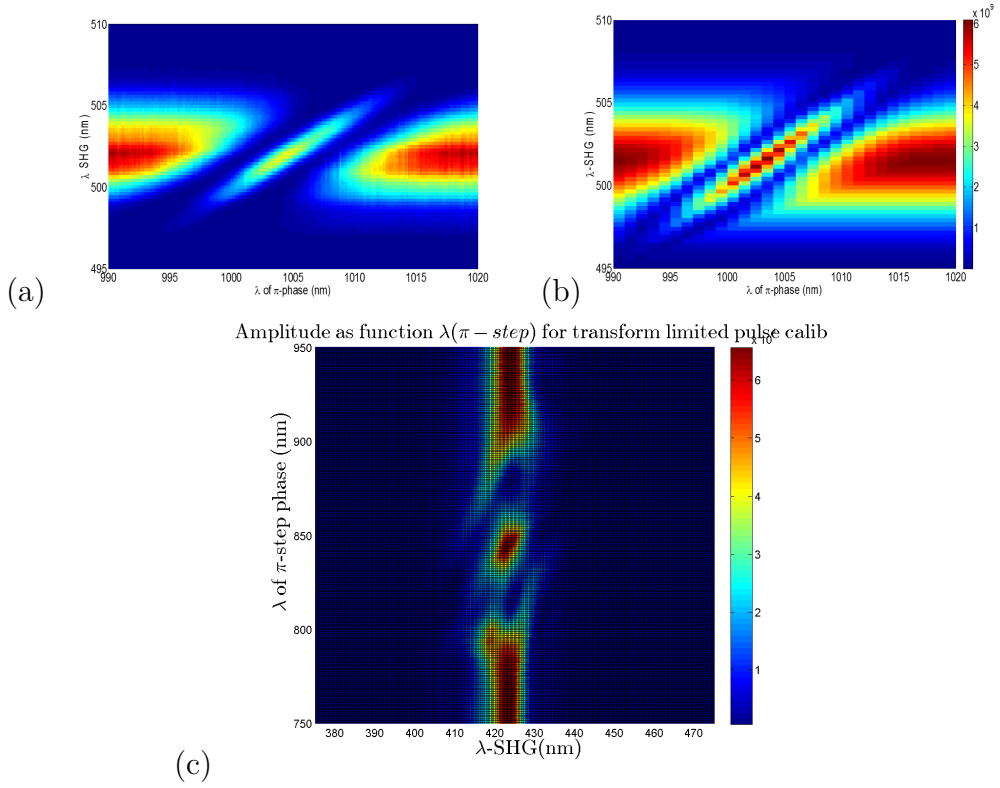

Figure 4.6: (a) Measured SHG from KTP crystal as function of π-step phase wavelength for a transform-limited pulse ($\lambda_{center} = 1003nm$), (b) Theoretical SHG calculation of the pulse from (a), (c) The same as (a) but with a broadband laser on BBO crystal

4.3 Analysis and prediction of ultrafast non-instantaneous interaction

Ultrafast light-matter interactions can be divided into two categories: instantaneous and non-instantaneouos. In the case of instantaneous interactions (e.g SHG in BBO crystal) there is no 'memory', which means that the interaction of the tail of the pulse is not affected by the leading part of the pulse. On the other hand, non-instantaneous interactions (e.g time dependent extinction cross-section of plasmonic systems) have 'memory'. Coherent control in these ultrafast processes can be achieved by employing shaped pulses. We show that by changing only the spectral phase of the incoming pulse, the spectral-spatial-temporal domains of the NS internal dynamic can be manipulated.

4.3.1 Optimizing SHG in plasmons using phase-shaping

Increasing optical nonlinearity in plasmonic nanostructures can be done using coherent control techniques similar to those used for increasing TPA in atomic physics, as described

in the following paragraphs.

In atomic system, it was assumed the pulse duration to be considerably shorter than all lifetimes involved in the interaction (the atom spends $\sim 100fs$ at the intermediate level before absorbing a second photon). From second-order time dependent perturbation theory, by using the Fourier Transform (FT) of the pulse, assuming short time interaction ($t \approx 0$) and using 'Cauchy's integral formula', the contribution to the excited state amplitude due to a transition through an intermediate resonant level $|i\rangle$ is given by,

$$a_f^r \approx -\frac{1}{i\hbar^2}\mu_{fi}\mu_{ig}[i\pi E(\omega_{ig})\cdot E(\omega_{fg}-\omega_{ig}) + P\int_{-\infty}^{\infty}\frac{E(\omega)\cdot E(\omega_{fg}-\omega)}{\omega_{ig}-\omega}d\omega] \tag{4.19}$$

where, μ_{fi} and μ_{ig} are the dipole moment matrix elements with $|g\rangle, |i\rangle$ and $|f\rangle$ the ground, intermediate, and final levels. $\omega_{ij} \equiv \frac{\omega_i-\omega_j}{\hbar}$, P is the principal value of Cauchy, and the summation is performed over intermediate resonant states of the unperturbed atom. The factor of $\frac{1}{\omega_{ig}-\omega}$ means the larger the detuning is, the lower the probability the atom will stay at the intermediate level long enough to absorb a second photon. The spectral components below and above the resonance excite the system in phase and π out of phase, respectively. In order to maximize the integral, $P\int_{-\infty}^{\infty}\frac{E(\omega)\cdot E(\omega_{fg}-\omega)}{\omega_{ig}-\omega}d\omega$, one can compensate the phase mentioned by giving a π-step phase to the field , E, in respect to the resonance intermediate level. One should note that in case where $\omega_{ig} = \frac{\omega_{fg}}{2}$, TPA can not be increased beyond the transform-limited interaction.

Plasmonic system have also resonances, but with a much wider spectral width (Γ), as a result of high absorption. The phase term in the perturbation theory should be expanded with an absorptive part such that:

$$\begin{aligned}&(a)\ \omega_{ig} \rightarrow \omega_{ig} + i\Gamma_{eff}\\ &(b)\ iP\int_{-\infty}^{\infty}\frac{E(\omega)\cdot E(\omega_{fg}-\omega)}{\omega_{ig}-\omega}d\omega \Rightarrow i\int_{-\infty}^{\infty}\frac{E(\omega)\cdot E(\omega_{fg}-\omega)}{\omega_{ig}+i\Gamma_{eff}-\omega}d\omega\end{aligned} \tag{4.20}$$

where, $\omega_{ig} = \frac{\omega_{fg}}{2} = \omega_{res}$ and $\Gamma_{eff} = \frac{2\epsilon_2}{|\frac{\partial\epsilon_1}{\partial\omega}|}$ [3.16] for $\epsilon_{metal} = \epsilon_1 \pm i\epsilon_2$ ($\pm$ depending on the convention). Consequently, the π-step phase should be changed to a more smoothed phase because the system absorbs photons in a wider band. The additional phase that appears in the SHG integral expression is $\varphi(\omega) = arctg(\frac{\omega_{ig}-\omega}{\Gamma_{eff}})$ which can be partially compensated by inserting the opposite phase into the expression $E(\omega)\cdot E(\omega_{fg}-\omega)$ using a pulse-shaper for increasing the SHG, e.g $\varphi(\omega) = -arctg(\frac{\omega_{ig}-\omega}{\Gamma_{eff}})\,\omega \leq \frac{\omega_{SHG}}{2}$.

Numerical simulation results can be seen in Figure 4.7 for three different phases and three different ratios between the widths of the pulse and the extinction cross-section

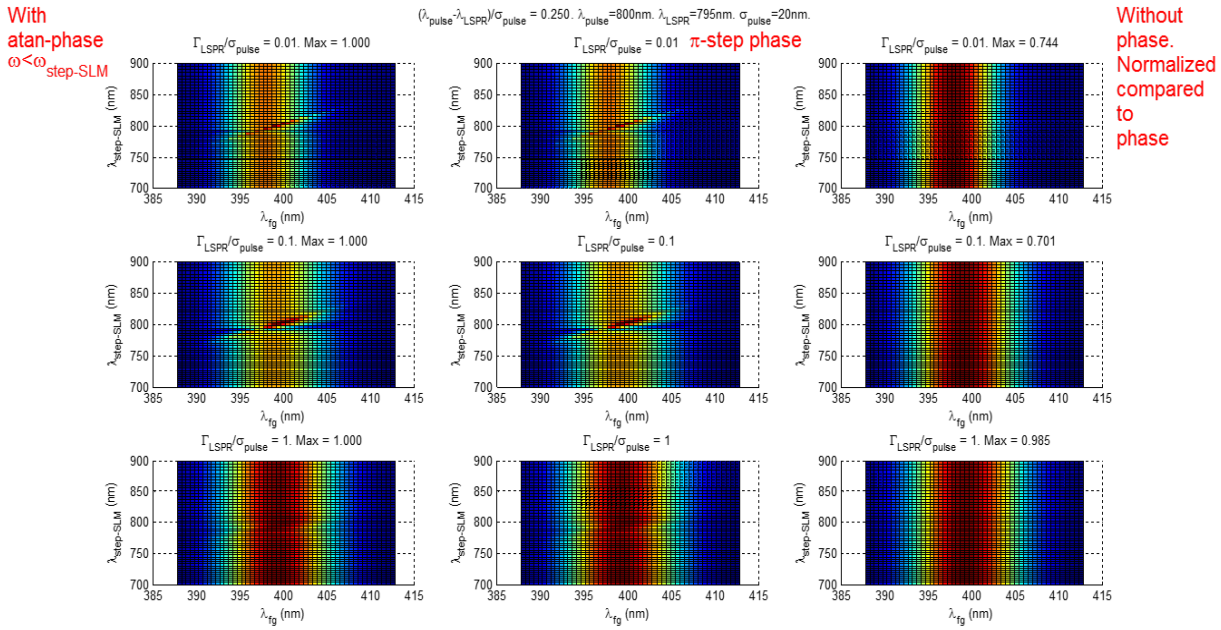

Figure 4.7: SHG spectrum intensity as function of λ_{step} for three different phases and three different ratios between the pulse width (σ_{pulse}) and the width of the extinction cross-section of the plasmonic system (Γ_{LSPR}). Left column is the arctg phase suggested above, $\varphi(\omega) = -arctg(\frac{\omega_{ig}-\omega}{\Gamma_{eff}})\,\omega \leq \frac{\omega_{SHG}}{2}$. The middle column is the $\pi - step$ phase case, as in the TPA case. The right column is a transform limited pulse with no phase. The rows, from top to bottom, display different ratios between the pulse width and the cross-section, $\frac{\Gamma_{LSPR}}{\sigma_{pulse}}$, 0.01, 0.1 and 1.

($\frac{\Gamma_{LSPR}}{\sigma_{pulse}}$). Each SHG amplitude ($a_f^r$) plot in the figure was made by calculating the a_f^r from Eq. 4.19 for a range of $\lambda_{step-SLM}$ and λ_{fg} (which stands for λ_{SHG} in our plasmonics system).

The main conclusion from the figure is that the coherent control for enhancing SHG would be seen only in the case of $0.1 \gtrsim \frac{\Gamma_{LSPR}}{\sigma_{pulse}}$ where an increase of only about 50% is seen in the calculations. The rule for $\frac{\Gamma_{LSPR}}{\sigma_{pulse}}$ determined here occurs in TPA where Γ_{LSPR} is very small in atomic systems.

In conclusion, we theoretically showed that wave-mixing in plasmonic systems can be increased by using techniques from atomic physics. We adjusted a coherent control technique for TPA to plasmonic system by inserting the effect of Γ_{LSPR} , the bandwidth of the plasmonic resonance. We expect the coherent control technique to significantly increase the wave-mixing only for the cases where the width of the LSPR is considerably small compared to the width of the incoming pulse. However, there is a doubt about the theory's quantitative predictions. The assumption that the pulse duration is considerably shorter than all lifetimes involved in the interaction doesn't comply as can be seen from the TTM. In the TTM, T_e changes significantly while the pulse is absorbs and causes a

shift in the resonance. But yet, we predict that the SHG will be increased by changing the transform-limited in an intelligent way. For higher order of wave mixing (i.e FWM or THG) a higher order of perturbation should be expanded so that the phase would be different and more complicated.

4.3.2 Coherent control of ultrafast dynamics in the two temperature model

Motivation

We show theoretically and through numerical simulations that we can control the ultrafast dynamics in a NS by only changing the phase of the pulse. The changes are analyzed by considering the maximum temperature of the electrons ($T_e - max$). The enhancement of T_e can be measured through the reflectance and transmission in a pump-probe setup.

Theoretical approach

As shown in the background, the coupled-equations for describing the TTM are [31]:

$$\begin{aligned}
&(a)\partial_t N(t) = -(\gamma_e + \gamma_l)N(t) + P_A(t) \\
&(b)C_e(t)\cdot\partial_t T_e(t) = -G(T_e - T_l) + \gamma_e N(t) \\
&(c)C_l(t)\cdot\partial_t T_l(t) = G(T_e - T_l) + \gamma_l N(t)
\end{aligned} \tag{4.21}$$

For understanding the ultrafast dynamics in plasmonic system, we will assume for simplicity (and for the physical correctness of energy conservation in the model) that the capacities and the coupling coefficient (C_e, C_l and G) are not temperature dependent which is not true in nature, yet is reasonable for our proof of concept analysis. By using Fourier's theorem ($\partial_t \to -i\Delta\omega$) and by defining $\Delta T = T_e - T_l$, it is easily shown that:

$$\begin{aligned}
&(a)\Delta T(\Delta\omega) = h_T(\Delta\omega)\cdot(\frac{\gamma_e}{C_e} - \frac{\gamma_l}{C_l})\tau_r\tau_{th}P_A(\Delta\omega) \\
&(b)h_T(\Delta\omega) = \frac{1}{1 - i\Delta\omega\tau_r}\cdot\frac{1}{1 - i\Delta\omega\tau_{th}} \\
&(c)\tau_r = \frac{C_eC_l}{C(C_e + C_l)} \\
&(d)\tau_{th} = (\gamma_e + \gamma_l)^{-1}
\end{aligned} \tag{4.22}$$

For intuition we can understand from Eq. (4.21) that the time factor τ_{th} stands for

the delay of the non-thermalized electrons transferring their energy, and the time factor τ_r is the delay of the thermalized electrons and lattice achieving equilibrium.

As we know from instantaneous interactions (e.g a SHG in BBO crystal), a transform limited pulse will generate the most powerful interaction. This is not the case in non-instantaneous interactions (e.g interaction of light with plasmonic systems) which is dictated by an ultrafast dynamics that can be modeled by the TTM model. For compensating the inherent phases of the plasmonic system a phase should be added to the incoming pulse ($P_A(\Delta\omega)$) for maximizing $\Delta T(\Delta\omega)$. The phase of the system is represented by $\varphi\{h_T(\Delta\omega)\}$, where $h_T(\Delta\omega)$ is the response function in the frequency domain in Eq. [4.22], such that:

$$\begin{aligned}
&(1) h_T(\Delta\omega) = \frac{1}{1 - i\Delta\omega\tau_r} \cdot \frac{1}{1 - i\Delta\omega\tau_{th}} \\
&(2) \varphi\{\frac{1}{1 - i\Delta\omega\tau_i}\} = arctg(\Delta\omega\tau_i) \\
&(3) \varphi\{A \cdot B\} = \varphi\{A\} + \varphi\{B\} \\
&(4) \Rightarrow \varphi\{h_T(\Delta\omega)\} = arctg(\Delta\omega\tau_r) + arctg(\Delta\omega\tau_{th})
\end{aligned} \tag{4.23}$$

where $-\pi \leq \varphi\{h_T(\Delta\omega)\} \leq \pi$.

In conclusion, by changing the pulse to be different from transform-limited which consequently lowers the peak power of the pulse, the overall effect on $\Delta T(\omega)$ will be more significant. This will influence dramatically the related nonlinear processes that are based on the electronic temperature, such as the thermal $\chi^{(3)}$ nonlinearity.

As can be understood intuitively and from the simulations, $\Delta T(\omega) \approx \Delta T_e(\omega)$ where $0.1 \gtrsim \frac{\Delta T_l(\omega)}{\Delta T_e(\omega)}$ because of the significant lattice's heat capacity and smaller scattering parameter, compared to the electrons. $\Delta T_e(t)$ can be measured as described in chapter (4.3.2) while considering the phenomena mentioned in chapter (3.2.1).

TTM of Plasmonic system- simulation

The simulation displays the time-dependent electronic and lattice temperatures, $T_e(t)$ and $T_l(t)$, respectively. The goal is to achieve a qualitative understanding and physical intuition about the temporal behavior of the ultrafast dynamics of light-matter interaction in plasmonic system.

The assumptions for our numerical simulations:

1. The field of the laser pulse ($E(\omega)$) is only absorbed through the LSPR ($\lambda_{laser} > \lambda_{ib}$). $P_{abs}(t) \sim F.T\{|E(\omega)|^2 \cdot \sigma_{abs}(\omega)\}$ where phases are also included in the $E(\omega)$ but not in the absorption cross-section ($\sigma_{abs}(\omega)$).

2. Femtosecond interaction: The simulation takes care of the first fs-ps until $T_e \sim T_l$ (until the electron's and lattice temperatures equilibrate). Consequently, diffusion from the NS to the environment is ignored.

3. σ_{abs} is simulated as time-independent. Generally, the plasmon's absorption cross-section depends on T_e and T_l and is analyzed very accurately in [16]. In the short time region ($<$ hundreds of fs) one can consider only T_e in the calculations.

4. We will keep the electron-phonon (e-ph) coupling ($G(T_e)$) and the electron heat capacity ($C_e(T_e)$) constant for simplicity in there value of about $T \approx 500^o K$. For completeness, we remark that in the literature the temperature dependent values were calculated up to temperature of $5 \cdot 10^4 K$ in [40]. In other models [16] [41] for small excitation ($T_e < 3000K$) $C_e(T_e) = aT_e$ where $a \sim 65[\frac{J}{m^3 K^2}]$ which seems to correlate with those values. Moreover, TTM with analytical expression for the values can be found in [42].

5. We use the electron-electron scattering coefficient $\gamma_e = \frac{1}{\tau_{e-e}}$ and the electron-phonon scattering coefficient $\gamma_l = \frac{1}{\tau_{e-ph}}$, where $\tau_{e-e} = 500fs$ and $\tau_{e-ph} = 1ps$ [43].

For a transform limited Gaussian pulse interacting with a nanobar of length $140nm$ and of width $40nm$ the interaction is shown in Figures 4.8 4.9.

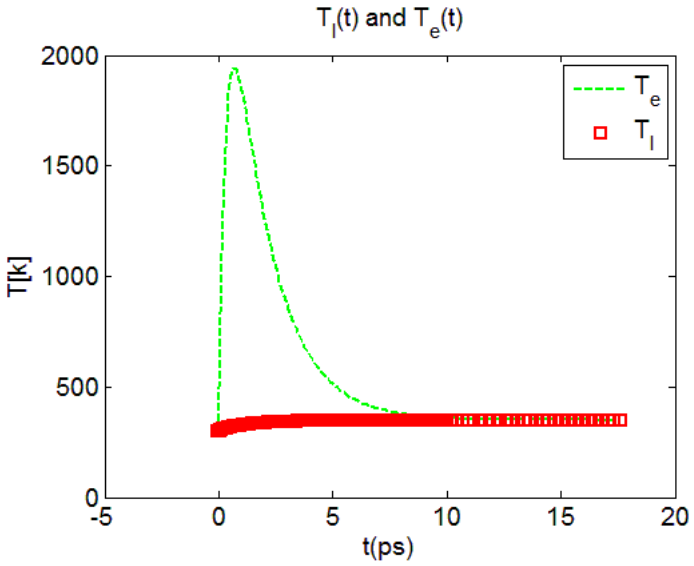

Figure 4.9: Example of interaction of a transform limited laser pulse with a NS. $T_e(t)$ and $T_l(t)$ as a function of time.

The maximum temperature of the electrons ($T_e - max$) in the presented TTM is about $2000K$. One can see that after a couple of ps the electrons and lattice thermalize, as expected. Comparing 3 different cases where only the pulse' spectral phase is changed

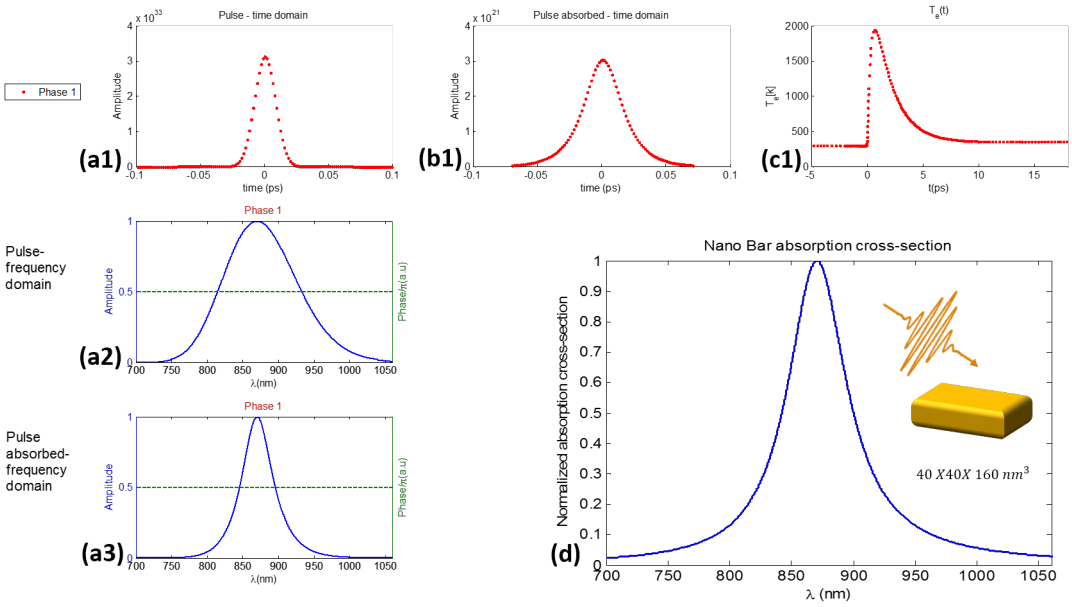

Figure 4.8: Simulated temporal and spectral response of a transform-limited pulse interaction with resonant plasmonic nanostructure. (a1) The pulse in the time domain. (a2) The absorbed power by the NS in the time. (a3) is the electrons temperature, T_e, as function of time simulated by the TTM. (a2) and (a3) are the pulse and absorbed power in the frequency domain. (d) is the absorption cross-section of the nanobar.

can be seen in the next Figure 4.10. As can be seen in the figure, T_e increases significantly from about 2000^oK to 6000^oK . The change in phase seems to separate the pulse into two pulses in the time domain.

By analyzing many simulations with different arctangent-phase a thorough understanding of the phase effect can be achieved as can be seen in Figure 4.11.

The figure is displayed as a function of $\Delta\lambda$, where the spectral phase is defined by:

$$\begin{aligned} \omega_0 &= \frac{2\pi c}{\lambda_0} \\ \Delta\omega &= \frac{2\pi c}{\lambda_0^2}\cdot\Delta\lambda \\ \varphi(\omega) &= arctg(\tfrac{\omega-\omega_0}{\Delta\omega}) \end{aligned} \tag{4.24}$$

where c is the speed of light and λ_0 is the resonance wavelength. For $|\Delta\lambda| \gg \lambda_{FWHM}$, where λ_{FWHM} is the spectral bandwidth of the incoming pulse, the pulse is actually transform-limited, while for $|\Delta\lambda| \ll \lambda_{FWHM}$ the phase is very similar to a $\pi - step$ behavior.

The results in figure [4.11] show that different spectral phases of the incoming pulse affect the ultrafast dynamics. The highest $T_e - max$ is achieved for $\frac{|\Delta\lambda|}{\lambda_{FWHM}} \approx \frac{0.001}{50} = 2\cdot 10^{-5}$, which means that the maximum increment of T_e in the system is achieved by

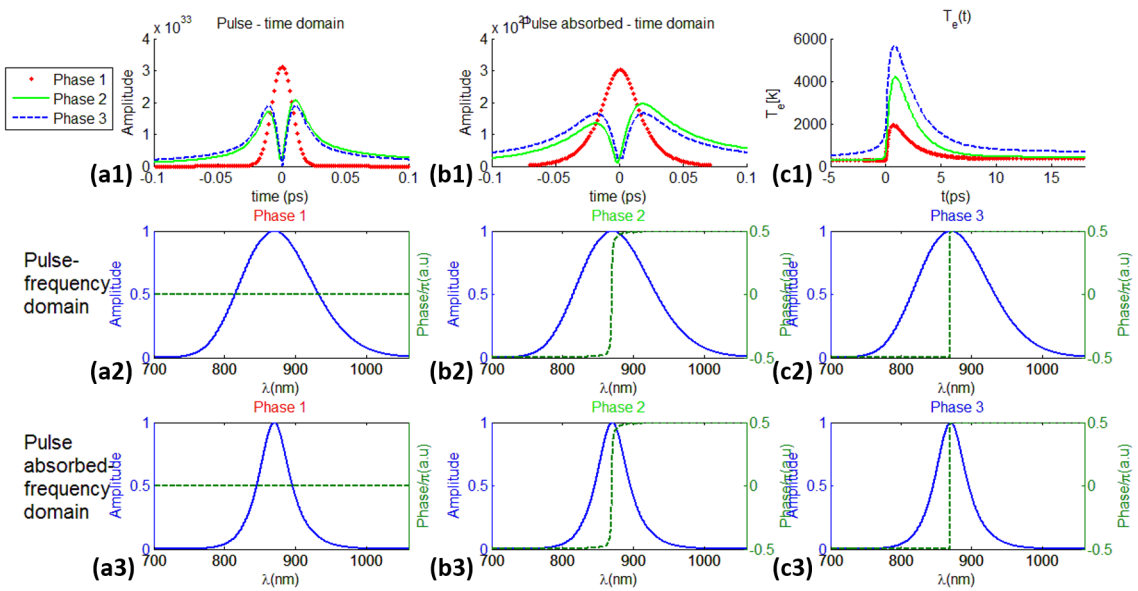

Figure 4.10: Comparison between TTM for 3 cases where only the phase is changed. (a1) Pulses in the time domain. (a2) Absorbed power by the NS in the time domain. (a3) Electrons temperature, T_e, as function of time, simulated by the TTM. The middle row, 2, and bottom row, 3, are the pulse and absorbed power in the frequency domain, respectively. Each column stands for a different phase, "Phase 1", "Phase 2" and "Phase 3".

a pulse which have a phase which is very similar to a $\pi - step$ phase, but is slightly different.

For summary, we studied the inherent non-linearity in the TTM using simulative and theoretical approach. It had been shown that the non-linearity can be measured through the spectral-phase relation between an incoming pulse and the temperatures, $\Delta T(t) = T_e(t) - T_l(t)$. The nonlinearity is caused by the non-instantaneous scattering time between the NTE, "hot-electrons" and the lattice. The inherent spectral-phase in the system can be intuitively understood as wavelength dependent time delay relation between the incoming pulse and ΔT. By shaping the spectral-phase of the incoming pulse the inherent phase of the TTM can be canceled and thus ΔT is maximized. T_e will probably not increase to such high temperature in real experiments as shown in the figures because the temperature dependent capacities of the electrons and lattice and more high-temperature effects were not taken into consideration. The change in T_e can be measured, e.g. in pump-probe experiment, through the changes in the electrical and optical properties.

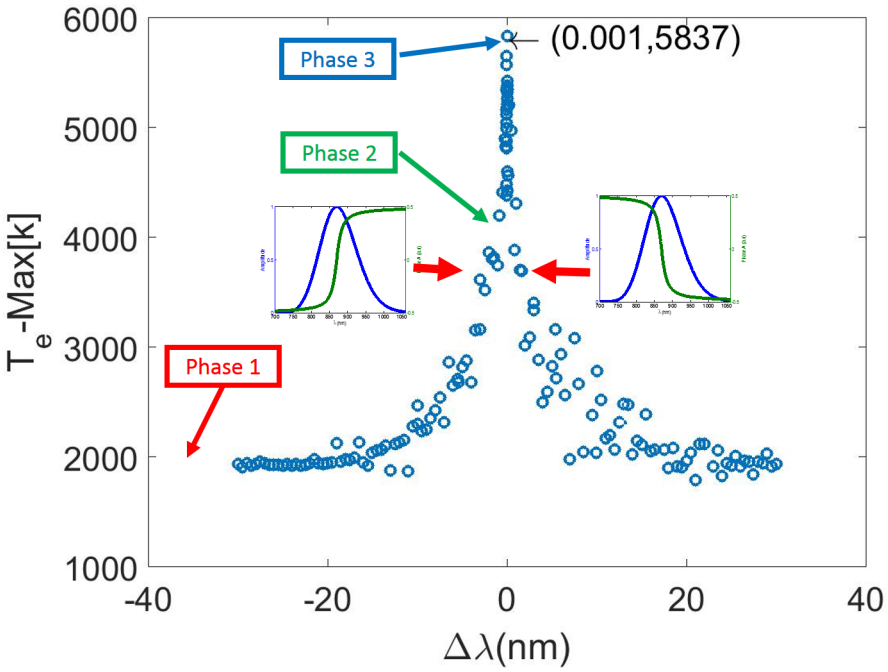

Figure 4.11: $T_e - max$ as function of $\Delta\lambda$, where $\Delta\lambda$ defines the arctg-phase of each pulse and $T_e - max$ is the maximum temperature calculated in the TTM simulation for the corresponding case. Phase 1-3 in the figure correspond to the phases from Figure 4.10.

Experimental consideration

When performing a pump-probe experiment on a NS the measured values are the transmission (or reflection) and is theoretically equals $\frac{\Delta T}{T} \approx \frac{\Delta\sigma_{ext}(T_e,\lambda)}{S}$ [16]. The change in the transmission can be seen also on metallic films without a NS.

To understand the connection between the measurements and the TTM one should understand also the experimental setup tools.

The pump electric field is modulated in the AOM with a frequency ω_m. A lock-in amplifier reads the transmission signals that are modulated by harmonies of ω_m. For the first hundreds of fs mostly the pump's energy is absorbed by the electrons so that:

$$\int\int \sigma_{abs} \cdot |E|^2 d\lambda dt = P_{abs} \approx \int_{T_0}^{T_{Max}} C_e(T_e) \cdot T_e dt \tag{4.25}$$

where $C_e \approx \gamma T_e, \gamma \sim 65[\frac{J}{m^3 K^2}]$. If we assume that the electric field E is modulated by the lock-in amplifier: $E \sim e^{i\omega_m t}$, $=> E^2 \sim T_e^2 => T_e \sim e^{i\omega_m t}$. The assumption that T_e is modulated needs to be thoroughly checked and can only be true when the absorbed power was mostly passed to the thermalized electrons. A similar conclusion is shown

in [44] and is used for example in [42].

In our case, we can assume that most of the energy is absorbed by the electrons. Consequently, we can expand C_e using Taylor expansion $C_e(T_e) \approx C_e(T_0) + \frac{\partial C_e}{\partial T_e}(T_e - T_0) + \frac{\partial^2 C_e}{\partial T_e^2}(T_e - T_0)^2 + ... , \frac{\partial C_e}{\partial T_e} \approx \gamma... .$

Define $f(T_e(t))$ as the energy absorbed by the electrons. If we continue analyzing the short time scale of the EM interaction where the electrons hold most of the energy, $f(T_e(t))$ as a function of time can be written as:

$$\begin{aligned} f(T_e(t)) &= C_e(T_e) \cdot T_e \\ f(T_e(t_f)) &= f(T_e(0)) + \int_0^{t_f} \frac{df(T_e(t))}{dT_e} \cdot \frac{dT_e}{dt} dt \\ &= f(T_e(0)) + \int_0^{t_f} [\frac{dC_e(T_e)}{dT_e} T_e + C_e(T_e)] \cdot \frac{dT_e}{dt} dt \end{aligned} \tag{4.26}$$

where the modulated values have different orders of T_e and consequently different orders of modulations in the measurement. For evaluating the transmission or reflection for different modulations orders, one needs to find $\Delta\sigma_{ext}(T_e, \lambda)$ which can be estimated by using the temperature dependent characteristic of the NS metal, $[\epsilon_1(T_e), \epsilon_2(T_e)]$ or $[\omega_p(T_e), \gamma(T_e)]$.

5 Summary and outlook

In this thesis, I have merged theories of extreme spatio-temporal resolution at the IR optical regime, in order to study ultrafast phenomena at nanoscale resolution via coherent control methods.

I have presented a theoretical approach which estimates the effect of thin layers on plasmon resonance. These estimations were successfully verified with experimental results in the case of ITO adhesion layer which is in use in the fabrication process. Moreover, the model was used to estimate the effect of MoS_2 thin layer on LSPR of a gold nanostructure in water.

Moreover, I presented mathematical approaches and simulations of coherent control in plasmonics system. The first approach is a coherent control manipulation for increasing SHG in plasmonic system. The model is based on the theory of coherent quantum control of two photon absorption (TPA) in atomic physics. In the second approach I showed that the ultrafast dynamics of plasmonic system can be controlled by the phase of the pulse which interact with the system. The approach is base on the Two Temperature Model (TTM) and the performance is measured by the enhancement of the T_e peak.

If the theories proves successful, a thorough understanding of the temporal-spectral effects in the ultrafast dynamics in plasmonic system could be achieved. The mentioned manipulations can help in understanding nonlinearities which Boyd mentioned [28] as "reported values of this quantity span a range of more than three orders of magnitude". Moreover, some thorough articles explained the phase effect of the TTM in a different way from the thesis [31], "As a consequence of the delay, blue-shifted frequency components are suppressed, while red-shifted components are amplified". By experiment I will verify my prediction against the quoted prediction.

We plan to check the predictions by experiments using a spectral phase controlled pulse using the pulse-shaper. An experiment of increasing nonlinearity of wave-mixing in plasmonics system will be done with a laser with wavelengths over $1.5\mu m$ which the Third Harmonic Generation (THG) and SHG would only slightly be absorbed in gold overcoming the interband absorption. Another experiment will be done by controlling the laser phase in a pump-probe setup where we expect to see variations of the pump-probe profile corresponding to phase manipulations. We expect that the realization

of such enhanced nonlinearity from plasmonic nanostructure will allow to realize many applications, such as nonlinear sensors and nonlinear spectroscopy.

The theory could be further developed to explain the formation of nonlinear wave-mixing in plasmonic systems in a femtosecond timescale. This development should combine the temperatures evolution and the nanostructure geometrical effects.

6 Appendix: Extension of perturbation approach on LSPR an its applications

6.1 Motivation

In this chapter, I developed some theories for matching experimental results which have some differences from the basic Effective Medium Theory (EMT). Some of the theoretical results were used in submitted paper.

The motivation for finding a model for describing the influence of thin layers appeared while trying to match measurements of NS transmission spectrum, Comsol simulations and MGT. We expected for Lorentzian shape resonances while in practice we got non-Lorentzian shape resonances in the wavelength range of $\gtrsim 1200nm$, which happens because the ITO starts to be absorptive at those wavelengths. Moreover, the measurements didn't fit the Comsol simulations I have done for Au NS with a wavelength independent medium and also for guesses of wavelength dependent medium.

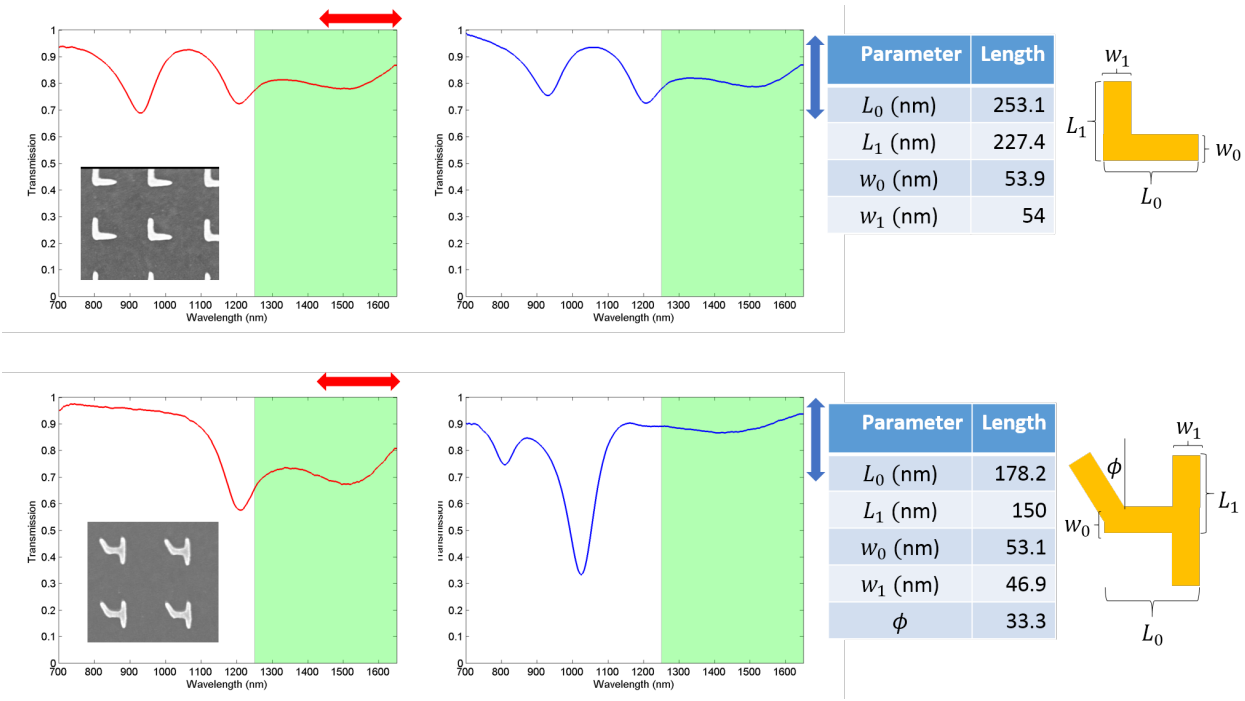

Figure 6.1: Two Au NSs over a Silica coated with a thin layer of ITO and their spectrums in the X and Y polarizations. The colored area in the graphs is the problematic wavelengths range in the measurements.

6.2 Fraction of adhesion layer and the medium permittivity

As shown above in Eq. [3.17], the resonance wavelength (λ_{LSPR}) behavior of a metallic ellipsoid with a small imaginary permittivity part ($\epsilon_1 \gg \epsilon_2$) in a dielectric medium [16] is described by:

$$\lambda_{LSPR} = \lambda_p \cdot \sqrt{\epsilon_1^{ib}(\lambda_{LSPR}) + \frac{1-L_i}{L_i} \cdot \epsilon_{medium0}} \approx \lambda_p \cdot \sqrt{\frac{1-L_i}{L_i} \cdot \epsilon_{medium0}} \tag{6.1}$$

where $\epsilon_{medium0}$ is the medium permittivity and $\epsilon_1^{ib}(\lambda_{LSPR})$ could be neglected far from the interband resonance. The approximation was shown to work in the literature and in Comsol simulations we have done for many geometries.

It has also been shown in Eq. [3.19] that:

$$\frac{\omega - \omega_0}{\omega_0} \approx -\frac{f}{2} \cdot \frac{\epsilon_{adh} - \epsilon_{medium0}}{\epsilon_{medium0}} \tag{6.2}$$

The outcome of combining the two equations is:

$$-\frac{f}{2} \cdot \frac{\epsilon_{adh} - \epsilon_{medium0}}{\epsilon_{medium0}} \approx \frac{\omega - \omega_0}{\omega_0} = \frac{\frac{1}{\lambda_{SPR}} - \frac{1}{\lambda_{SPR0}}}{\frac{1}{\lambda_{SPR0}}} = \frac{\lambda_{SPR0}}{\lambda_{SPR}} - 1 = \sqrt{\frac{\epsilon_{medium0}}{\epsilon_{medium}}} - 1 \tag{6.3}$$

where $\epsilon_{medium0}$ and ϵ_{medium} are the medium permittivity before and after adding the adhesion layer.

$$\begin{aligned} &1 - \frac{f}{2} \cdot \frac{\epsilon_{adh} - \epsilon_{medium0}}{\epsilon_{medium0}} \approx \sqrt{\frac{\epsilon_{medium0}}{\epsilon_{medium}}} \rightarrow \epsilon_{medium} = \frac{\epsilon_{medium0}}{(1 - \frac{f}{2} \cdot \frac{\epsilon_{adh} - \epsilon_{medium0}}{\epsilon_{medium0}})^2} = \\ &= (|\frac{f}{2} \cdot \frac{\epsilon_{adh} - \epsilon_{medium0}}{\epsilon_{medium0}}| \ll 1) = \\ &= \epsilon_{medium0} \cdot (1 + f \cdot \frac{\epsilon_{adh} - \epsilon_{medium0}}{\epsilon_{medium0}}) \end{aligned} \tag{6.4}$$

The last assumption should be carefully used and must be checked for thin layers which are not extremely thin and where $1 \ll \frac{\epsilon_{adh}}{\epsilon_{medium0}}$ for the relevant wavelength range.

Finally we get:

$$\epsilon_{medium} \approx \epsilon_{medium0} \cdot (1 + f \cdot \frac{\epsilon_{adh} - \epsilon_{medium0}}{\epsilon_{medium0}}) \tag{6.5}$$

And more precisely, we should note that in our measurements the adhesion takes over part of the SiO2 place and $\Delta\epsilon$ needs to be calculated by:

$$\epsilon_{medium}(\lambda) \approx \epsilon_{medium0} \cdot (1 + f \cdot \frac{\epsilon_{adh}(\lambda) - \epsilon_{SiO2}}{\epsilon_{medium0}}) \tag{6.6}$$

In experimental realization, $\epsilon_{medium0} = \frac{\epsilon_{SiO2}+\epsilon_{ALR}}{2}$ [45] and $\epsilon_{adh}(\lambda)$ is wavelength dependent due to the ITO is the adhesion layer, .

It can be easily seen that for a very thin layer there is a linear relation between the layer's thickness and the medium's effective permittivity:

$$\Delta\epsilon_{medium}(\lambda) \approx f \cdot (\epsilon_{adh}(\lambda) - \epsilon_{SiO2}) \tag{6.7}$$

This result is trivial and could be intuitively deduce from [45] when approximating no effect from the inclusion. On the other hand, it is not accurate [45].

If we assume an exponential decay-length, x_0 , of the field from the NS, the change of the medium permittivity is:

$$\begin{aligned}\Delta\epsilon_{medium}(\lambda, d) \approx \{\Delta\epsilon = (\epsilon_{adh}(\lambda) - \epsilon_{SiO2})\} = 0.5 \cdot \frac{\int_0^d \Delta\epsilon \cdot exp[-x/x_0]dx}{\int_0^\infty exp[-x/x_0]dx} = \\ = 0.5 \cdot \Delta\epsilon \cdot (1 - exp[-d/x_0])\end{aligned} \tag{6.8}$$

where d is the width of the thin-layer.

6.3 New perturbative approach for calculations of thin layer effect on LSPR and its application on MoS_2 layers

In my research, I have developed a new model for calculating the effect of thin layer on the LSPR based on the theory described in Eq. [3.19], where the original model seems to have some critical wrong assumptions as mentioned above.

The new model will be checked on a case of thin MoS_2 shell-layer with $h = 0.65nm$[1] coating a spherical gold NS with $radius = 5nm$.

The assumptions of the original perturbative approach [23] for calculation of thin layer influence on LSPR should be fixed for our MoS_2 case:

1. The resonance wavelength of Au NS in water is $\lambda_{res} = 515nm$ and for Au NS with a thin layer of MoS_2 in water $\lambda_{res} = 957nm$ as can be seen in figure [6.2] (where simulations of Au NP in MoS_2 medium showed LSPR of about $1000nm$). One can see that the LSPR's shift is significant, so that the approximation $\frac{\omega-\omega_0}{\omega_0} \approx \frac{\omega-\omega_0}{\omega}$ made in the original article can't be done.

2. We will still assume that the electric field doesn't change much in the relevant volume in the cases with and without the thin MoS_2 coating.

3. The fraction of MoS_2, f, will be calculate as the part of the MoS_2 thin layer shell from the 'relevant volume' where 'relevant volume' is where the fields interact and should be taken as $R_{relevant-volume} \approx depthFactor \cdot R_{Au}$, $depthFactor \lesssim 1.4$ [21]. This assumption is only partially right as the materials near the NS surface affect the medium more than other parts of the medium because of the decay of the plasmon's fields.

4. The permittivity of MoS_2,$\epsilon_{MoS_2}(\lambda)$, will be inserted to the equations as wavelength dependent [46].

Consequently, the new equation for the LSPR calculation is:

$$\frac{\omega - \omega_0}{\omega} = -\frac{f}{2} \cdot \frac{\epsilon_{MoS_2}(\omega) - \epsilon_{H_2O}}{\epsilon_{H_2O}} \tag{6.9}$$

and can be easily solved numerically.

The results give $\lambda_{res}(depthFactor \approx 1.4) = 932nm$, $\lambda_{res}(depthFactor \approx 1.35) = 970nm$, $\lambda_{res}(depthFactor \approx 1.3) = 1012nm$ which show a good approximation to the measured data.

[1] Synthesized and characterized by Anna Lutin Department of Materials and Interfaces Weizmann Institute of Science , and is being researched by Dr. Lena Yadgarov

(a) 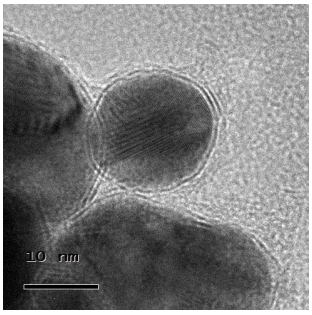

(b) 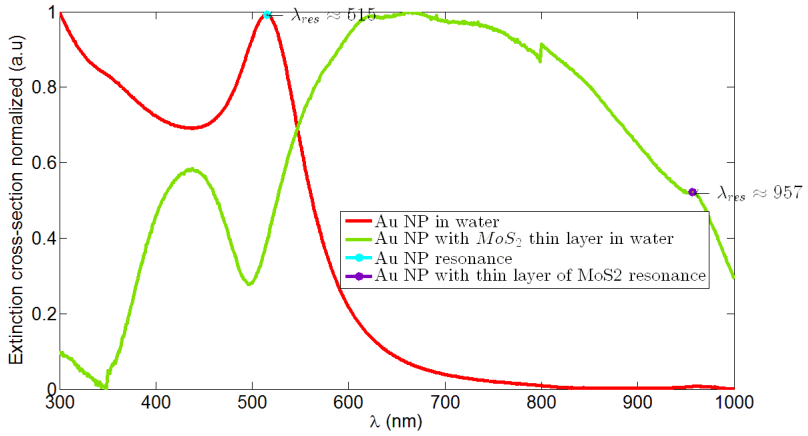

Figure 6.2: (a) TEM of Au NS with thin layer of MoS_2 (b) Extinction cross-section of Au NS in water and Au NS with MoS_2 layer in water

Although we have experimental result, a more thorough comparison of the model to experiments must be done before taking it for gospel. The results should be checked using Comsol simulations for variety of cases with changes in the width of the layer.

6.4 Deep Learning for Design and Retrieval of Nano-photonic Structures

6.4.1 Motivation

This project concentrate on breaking the diffraction limit in Plasmonics nanoscale sub-wavelength systems using Deep-Learning (DL) and is a result of a collaboration of a number of researchers in our 'Femto-Nano' group and the DL group. DL is a branch of machine learning rebranding 'neural networks' which attempts to mimic the activity in layers of neurons in the neocortex.

The goal of the research was to suggest a proven technique to easily retrieve or design a NS with a desirable spectrum as can be seen in figure [6.3]. NS's spectrum have high nonlinear dependency on the geometry parameters and consequently mostly don't have any analytical model for the calculation.

6.4.2 Theoretical approach for measurements compatibility

NS are fabricated over a glass with ITO adhesion layer. Compatibility between measurements and Comsol simulations of LSPR spectrum was achieved when we used a $100nm$ coating thickness made in the Technion where it's imaginary (absorptive) part of

the refractive index could be neglected up to $2\mu m$ and the wavelength dependent $\epsilon_{ITO}(\lambda)$ was given.

The surroundings permittivity (ϵ_d) was calculated by:

$$\epsilon_d(\lambda) = \frac{\epsilon_{ITO}(\lambda) + \epsilon_{AIR}}{2} \tag{6.10}$$

neglecting the effect from the inclusion, which is not accurate [5, 45]. The SiO_2 could be neglected because the thickness of the ITO layer is $100nm$ and the NS thickness is $40nm$ were consequently, the plasmon's induced fields decay length are much shorter than the ITO coating thickness.

My parts in the project, additional to the brainstormings, were:

1. Producing the Comsol simulations.
2. Taking part in measuring the transmission spectrum of the fabrications.
3. Calibrating the Comsol simulation to the measurements overcoming the ITO layer effect on the LSPR as described in equation [6.10], which was used in the case of resonances in the range of long wavelengths of our measurements.
4. Analyzing the Comsol and fabrications results.

6.4.3 The research and results

At the beginning, many Comsol simulations of transmission spectrum were calculated and organized into a dataset for the DL group to build the DL-network. Afterwards measured transmission spectrums where inserted to the network for revealing the sub-wavelength NSs. The suggested geometries where simulated in Comsol and afterwards fabricated for measuring there actual transmission spectrums. The DL results matched the simulations and fabrication in a very good accuracy up to fabrication resolution issues (thickness and roundness of the NS) for the upper range of the wavelengths.

The theoretical approach for the measurements compatibility with the simulations, as explained above, was important for the proof of concept for the ability of fabricating on demand NS and retrieving a real NS spectrum.

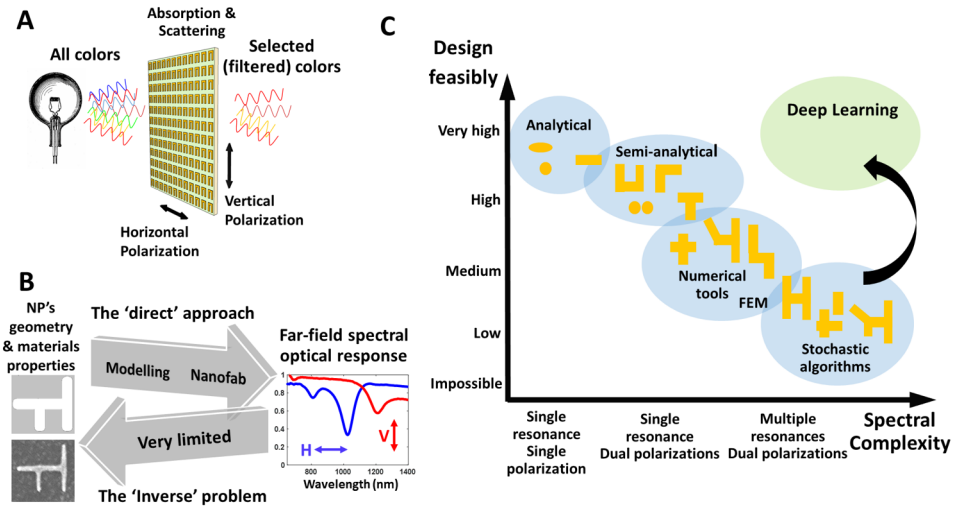

Figure 6.3: Deep learning Nano-photonics and the 'inverse' problem (A) Interaction of light with plasmonic nanostructures. Incoming electromagnetic radiation interacts with man-made sub-wavelength structures in a resonant manner, ultimately leading to an effective optical response where the optical properties for both polarizations of the designed metamaterial are dictated by the geometry at the nanoscale rather than the chemical composition. (B) To date, the approach enabled by the computational tools available only allow for a 'direct' modeling i.e. predicting the optical response in both polarization of a nanostructure based on its geometry, constituent and surrounding media. However, the 'inverse' problem, where the tool outputs a nanostructure for a input desired optical response, is much more relevant from a designer point of view and currently unachievable in a time efficient way. The more complex the optical response desired, the more unattainable is the solution of the inverse problem (C). The deep learning approach bridges this gap and unlocks the possibility to design, at the single nanoparticle level, complex optical responses with multiple resonances and for both polarizations.

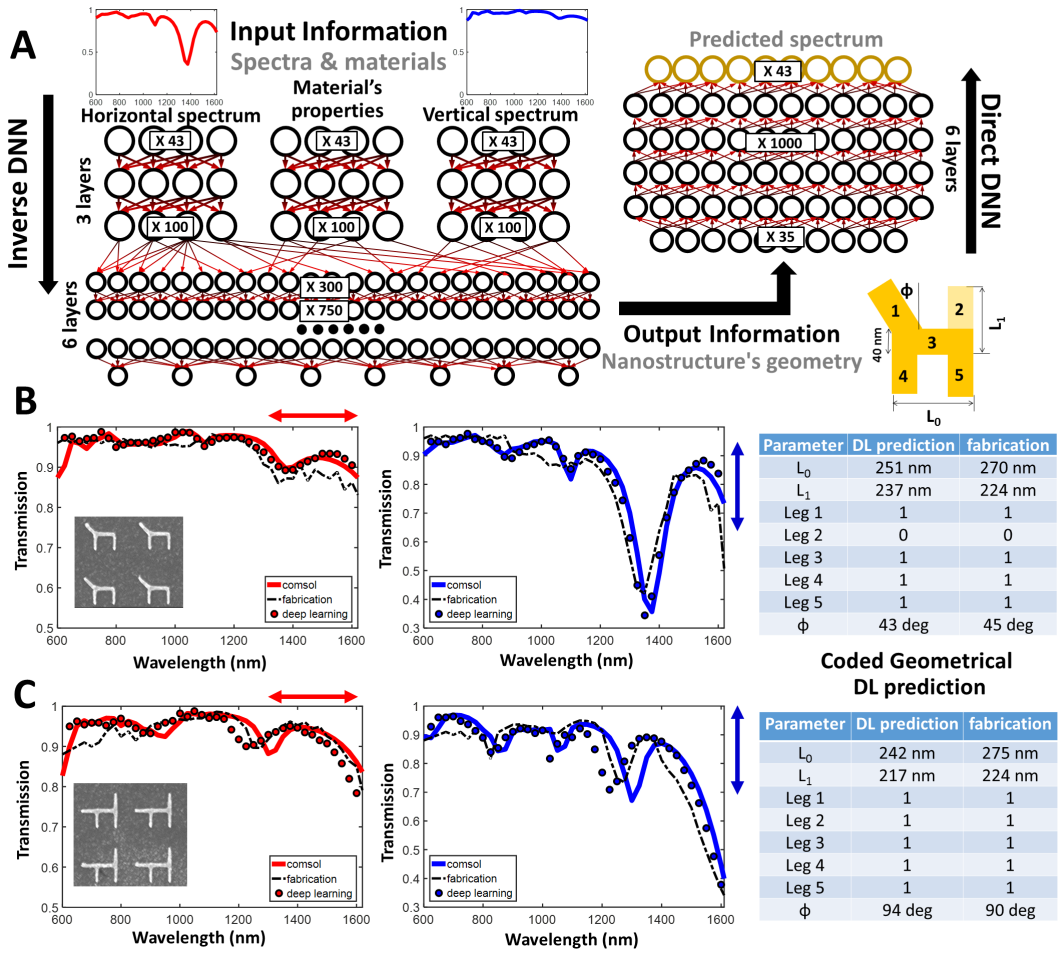

Parameter	DL prediction	fabrication
L_0	251 nm	270 nm
L_1	237 nm	224 nm
Leg 1	1	1
Leg 2	0	0
Leg 3	1	1
Leg 4	1	1
Leg 5	1	1
ϕ	43 deg	45 deg

Parameter	DL prediction	fabrication
L_0	242 nm	275 nm
L_1	217 nm	224 nm
Leg 1	1	1
Leg 2	1	1
Leg 3	1	1
Leg 4	1	1
Leg 5	1	1
ϕ	94 deg	90 deg

Figure 6.4: Deep learning architecture and retrieval of nanostructure's geometry. (A) The Deep networks have a cascaded structure of many layers of nonlinear processing units, where each layer uses the output from the previous layer as input. The network had an unusual structure as can be seen in the article. The input of the network was the X and Y polarization spectrums and the output was the subwavelength NS. We run a COMSOL simulation with the predicted NS. The results of this process for the two different nanostructures we have fabricated are depicted in (B) and (C). The measured spectrum is depicted in a red (blue) dotted line for the horizontal (vertical) input polarization. The DL predicted geometry is represented by the different lengths in the table. The DL spectrum based on the predicted geometry is depicted as full circles. The results of the COMSOL simulations based on the DL predicted geometry are represented as full lines.

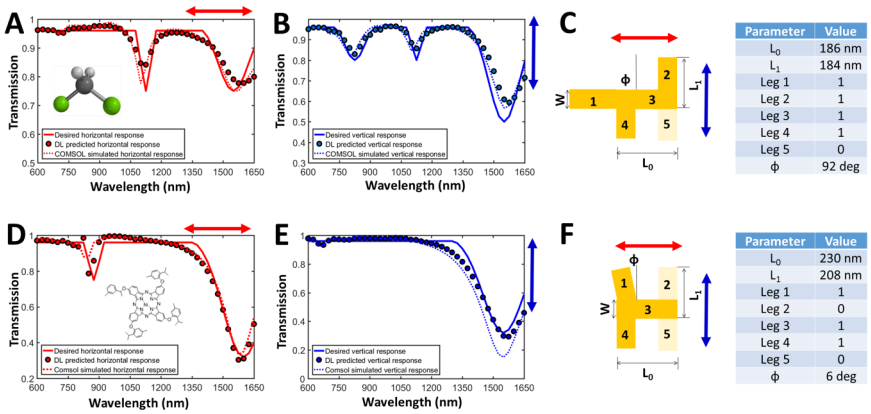

Figure 6.5: Prediction of the nanostructure's geometry for chemical sensing. (A-C) DNN based design of a gold plasmonic structure targeted to the organic molecule Dichloromethane with different spectral polarization response (A-B) on one polarization axis. It has two resonances on 1150nm and a broad one between 1400-1600nm, whereas on the orthogonal polarization, it has three resonances, at around 820 nm (match a Ti:Sapphire femtosecond laser excitation for a pump-probe experiment), 1064nm and 1550nm (C) Configuration and dimensions of the plasmonic structure found by the DNN. (D-E) The targeted molecule is asymmetrical Phthalocyanine dimer 1a, a synthetic molecule which has more complex polarization characteristics, with potential applications due to its charge transfer properties. (F) Configuration and dimensions of the plasmonic structure found by the DNN. In both geometries, after prediction of the geometry, COMSOL numerical simulations were performed, showing an excellent agreement with the desired spectra. This design approach can be extended to other molecules for biology, chemistry or material sciences.

Bibliography

[1] Mark L Brongersma, Naomi J Halas, and Peter Nordlander. Plasmon-induced hot carrier science and technology. *Nature nanotechnology*, 10(1):25–34, 2015. 1, 15

[2] Lukas Novotny. Effective wavelength scaling for optical antennas. *Physical Review Letters*, 98(26):266802, 2007. 2

[3] Aurélien Crut, Paolo Maioli, Natalia Del Fatti, and Fabrice Vallée. Optical absorption and scattering spectroscopies of single nano-objects. *Chemical Society Reviews*, 43(11):3921–3956, 2014. 3, 7

[4] Robert W Boyd. *Nonlinear optics*. Academic press, 2003. 3, 7

[5] Wenshan Cai and Vladimir M Shalaev. *Optical metamaterials*, volume 10. Springer, 2010. 3, 4, 7, 43

[6] Sujit Kumar Ghosh and Tarasankar Pal. Interparticle coupling effect on the surface plasmon resonance of gold nanoparticles: from theory to applications. *Chemical reviews*, 107(11):4797–4862, 2007. 3

[7] D. Polder and J.H. van Santeen. The effective permeability of mixtures of solids. *Physica*, 12(5):257 – 271, 1946. 3

[8] Wikipedia. Polarizability — wikipedia, the free encyclopedia, 2016. [Online; accessed 30-October-2016]. 5

[9] Wikipedia. Electric dipole moment — wikipedia, the free encyclopedia, 2016. [Online; accessed 23-September-2016]. 6

[10] Wikipedia. Polarization density — wikipedia, the free encyclopedia, 2016. [Online; accessed 24-September-2016]. 6

[11] Viktor Myroshnychenko, Jessica Rodríguez-Fernández, Isabel Pastoriza-Santos, Alison M Funston, Carolina Novo, Paul Mulvaney, Luis M Liz-Marzán, and F Javier Garcia de Abajo. Modelling the optical response of gold nanoparticles. *Chemical Society Reviews*, 37(9):1792–1805, 2008. 7

[12] CRAIG F Bohren and DONALD R Huffman. Absorption and scattering of. *Light by Small Particles*, page 209, 1983. 7

[13] Michael Quinten. *Optical properties of nanoparticle systems: Mie and beyond*. John Wiley & Sons, 2010. 7

[14] Gregory V Hartland. Optical studies of dynamics in noble metal nanostructures. *Chemical reviews*, 111(6):3858–3887, 2011. 7, 8, 15, 16

[15] Richard W Taylor, RubeÌĄn Esteban, Sumeet Mahajan, Roger Coulston, Oren A Scherman, Javier Aizpurua, and Jeremy J Baumberg. Simple composite dipole model for the optical modes of strongly-coupled plasmonic nanoparticle aggregates. *The Journal of Physical Chemistry C*, 116(47):25044–25051, 2012. 7

[16] Tatjana Stoll, Paolo Maioli, Aurélien Crut, Natalia Del Fatti, and Fabrice Vallée. Advances in femto-nano-optics: ultrafast nonlinearity of metal nanoparticles. *The European Physical Journal B*, 87(11):1–19, 2014. 8, 15, 31, 34, 39

[17] Application note- indium tin oxide. 9

[18] Wikipedia. Indium tin oxide — wikipedia, the free encyclopedia, 2016. [Online; accessed 26-October-2016]. 9

[19] Peijun Guo, Richard D Schaller, John B Ketterson, and Robert PH Chang. Ultrafast switching of tunable infrared plasmons in indium tin oxide nanorod arrays with large absolute amplitude. *Nature Photonics*, 2016. 9

[20] Zahirul M Alam, Israel De Leon, and Robert W Boyd. Large optical nonlinearity of indium tin oxide in its epsilon-near-zero region. *Science*, 352(6287):795–797, 2016. 9

[21] Basudev Lahiri, Rafal Dylewicz, M Richard, and Nigel P Johnson. Impact of titanium adhesion layers on the response of arrays of metallic split-ring resonators (srrs). *Optics express*, 18(11):11202–11208, 2010. 10, 41

[22] Jing Niu, Young Jun Shin, Jaesung Son, Youngbin Lee, Jong-Hyun Ahn, and Hyunsoo Yang. Shifting of surface plasmon resonance due to electromagnetic coupling

between graphene and au nanoparticles. *Optics express*, 20(18):19690–19696, 2012. 10, 12

[23] Claus Jeppesen, Niels Asger Mortensen, and Anders Kristensen. The effect of ti and ito adhesion layers on gold split-ring resonators. *Applied Physics Letters*, 97(26):263103, 2010. 10, 11, 41

[24] Wei-Shun Chang, Fangfang Wen, Debadi Chakraborty, Man-Nung Su, Yue Zhang, Bo Shuang, Peter Nordlander, John E Sader, Naomi J Halas, and Stephan Link. Tuning the acoustic frequency of a gold nanodisk through its adhesion layer. *Nature communications*, 6, 2015. 10

[25] Terefe G Habteyes, Scott Dhuey, Erin Wood, Daniel Gargas, Stefano Cabrini, P James Schuck, A Paul Alivisatos, and Stephen R Leone. Metallic adhesion layer induced plasmon damping and molecular linker as a nondamping alternative. *ACS nano*, 6(6):5702–5709, 2012. 10

[26] Wikipedia. Cavity perturbation theory — wikipedia, the free encyclopedia, 2016. [Online; accessed 2-October-2016]. 10

[27] Titus K Mathew. *Perturbation Theory- Encyclopedia of RF and Microwave Engineering*. 2005. 10

[28] Robert W Boyd, Zhimin Shi, and Israel De Leon. The third-order nonlinear optical susceptibility of gold. *Optics Communications*, 326:74–79, 2014. 13, 36

[29] Hatim Baida, Denis Mongin, D Christofilos, Guillaume Bachelier, Aurélien Crut, Paolo Maioli, Natalia Del Fatti, and Fabrice Vallée. Ultrafast nonlinear optical response of a single gold nanorod near its surface plasmon resonance. *Physical review letters*, 107(5):057402, 2011. 13, 14

[30] Lutz Waldecker, Roman Bertoni, Ralph Ernstorfer, and Jan Vorberger. Electron-phonon coupling and energy flow in a simple metal beyond the two-temperature approximation. *Physical Review X*, 6(2):021003, 2016. 15

[31] Andrea Marini, Matteo Conforti, Giuseppe Della Valle, Ho Wai Howard Lee, Tr X Tran, Wonkeun Chang, Markus A Schmidt, Stefano Longhi, Philip St J Russell, and Fabio Biancalana. Ultrafast nonlinear dynamics of surface plasmon polaritons in gold nanowires due to the intrinsic nonlinearity of metals. *New Journal of Physics*, 15(1):013033, 2013. 15, 29, 36

[32] Jose Casas-Vázquez and David Jou. Temperature in non-equilibrium states: a review of open problems and current proposals. *Reports on Progress in Physics*, 66(11):1937, 2003. 16

[33] Taeho Shin, Samuel W Teitelbaum, Johanna Wolfson, Maria Kandyla, and Keith A Nelson. Extended two-temperature model for ultrafast thermal response of band gap materials upon impulsive optical excitation. *The Journal of chemical physics*, 143(19):194705, 2015. 16

[34] Wikipedia. Pulse shaping — wikipedia, the free encyclopedia, 2015. [Online; accessed 12-April-2015]. 18

[35] JENOPTIK-Optical Systems. Slm-s640d usb, slm-s320d usb, technical documentation. Technical report, 03 2015. 18, 19

[36] Dimitris Sofikitis, Sébastien Weber, Andréa Fioretti, Ridha Horchani, Maria Allegrini, Béatrice Chatel, Daniel Comparat, and Pierre Pillet. Molecular vibrational cooling by optical pumping with shaped femtosecond pulses. *New Journal of Physics*, 11(5):055037, 2009. 22

[37] Haim Suchowski, Adi Natan, Barry D Bruner, and Yaron Silberberg. Spatio-temporal coherent control of atomic systems: weak to strong field transition and breaking of symmetry in 2d maps. *Journal of Physics B: Atomic, Molecular and Optical Physics*, 41(7):074008, 2008. 23

[38] Doron Meshulach and Yaron Silberberg. Coherent quantum control of multiphoton transitions by shaped ultrashort optical pulses. *Physical Review A*, 60(2):1287, 1999. 23, 25

[39] Nirit Dudovich, Barak Dayan, Sarah M Gallagher Faeder, and Yaron Silberberg. Transform-limited pulses are not optimal for resonant multiphoton transitions. *Physical Review Letters*, 86(1):47, 2001. 25

[40] Zhibin Lin and Leonid Zhigilei. Electron-phonon coupling and electron heat capacity in metals at high electron temperatures. 31

[41] Ozgur Ekici, Richard K Harrison, Nicholas J. Durr, Dan Eversole, Myoungkyu Lee, and Adela Ben-Yakar. Thermal analysis of gold nanorods heated with femtosecond laser pulses. *Journal of physics D: Applied physics*, 41(18):185501, 2008. 31

[42] Lan Jiang and Hai-Lung Tsai. Improved two-temperature model and its application in ultrashort laser heating of metal films. *Journal of heat transfer*, 127(10):1167–1173, 2005. 31, 35

[43] Chi-Kuang Sun, F Vallée, LH Acioli, Erich P. Ippen, and James G. Fujimoto. Femtosecond-tunable measurement of electron thermalization in gold. *Physical Review B*, 50(20):15337, 1994. 31

[44] TQ Qiu, T Juhasz, C Suarez, WE Bron, and Chang-lin Tien. Femtosecond laser heating of mult-layer metals–ii. experiments. *Previews of Heat and Mass Transfer*, 1(21):2, 1995. 35

[45] Mario G Silveirinha and Carlos A Fernandes. Effective permittivity of a medium with stratified dielectric host and metallic inclusions. In *Antennas and Propagation Society International Symposium, 2004. IEEE*, volume 4, pages 3777–3780. IEEE, 2004. 40, 43

[46] A R Beal and Howard P Hughes. Kramers-kronig analysis of the reflectivity spectra of 2h-mos 2 , 2h-mose 2 and 2h-mote 2. *Journal of Physics C: Solid State Physics*, 12(5):881, 1979. 41

אוניברסיטת תל אביב

הפקולטה למדעים מדויקים ע"ש ריימונד ובברלי סאקלר

בית הספר לפיסיקה ואסטרונומיה

המחלקה לחומר מעובה

הגברת תופעות אופטיות לא לינאריות באמצעות שליטה בדינמיקה אולטרה מהירה במבנים פלזמוניים ננומטריים

חיבור זה מוגש כחלק מהדרישות לקבלת תואר 'מוסמך למדעים' באוניברסיטת תל אביב

על ידי

אחיה נגלר

עבודה זו הוכנה בהנחיתו של

ד"ר חיים סוכובסקי

נובמבר 2016

תקציר

חקרנו את השילוב בין העולמות של מבנים ננומטרים, תופעות של דינמיקה מהירה ושליטה קוהרנטית באמצעות אינטרקציה של אור וחומר.

חקרנו תופעות על מבנים ננומטרים באמצעות תיאוריה של פלזמונים והרחבתם לצורך התאמתם לניסויים שמתרחשים בפועל במעבדה. המודלים מסבירים תופעות שמתרחשות כתוצאה משכבה דקה הנוספת למערכת.

בנוסף, כתבנו תוכנות למכשירים הנחוצים לצורך חקירת תופעות אולטרה-מהירות מסדר גודל של פמטו ($1 \cdot 10^{-15}$) שניות, כגון FROG, SLM ועוד. השימוש ב- SLM חיבור ה-SLM הכריח אותי להבין את התופעות בהם משתמש המכשיר ואת המתמטיקה, כך שכעת ניתן לחבר את ה-SLM בקונפיגורציות מיוחדות. כיול ה-SLM נעשה באמצעות טכניקות של שליטה קוהרנטית כך ששינוי הפאזה של הפולס משפיע על ההרמוניה השנייה (SHG).

פיתחנו מספר מודלים שמסבירים תופעות שנוצרות כתוצאה משינוי פאזת הפולס במערכות פלזמוניות. החלק המרכזי של העבודה עסק בפיתוח סימולציית 'טמפרטורה של שתי רמות' (TTM) אשר מתארת את הדינמיקה המהירה במערכות פלזמוניות. באמצעות שליטה קוהרנטית, הראנו בסימולציה שניתן להשפיע על טמפ' האלקטרונים במערכת באמצעות שינויי פאזה בפולס בלבד. תופעה זו יכולה להימדד במעבדה באמצעות מערך pump-probe עם ה-SLM.